universidade de aveiro

Assimilate

Assessment of Seismic Safety Integrated with Machine Learning and Tremors

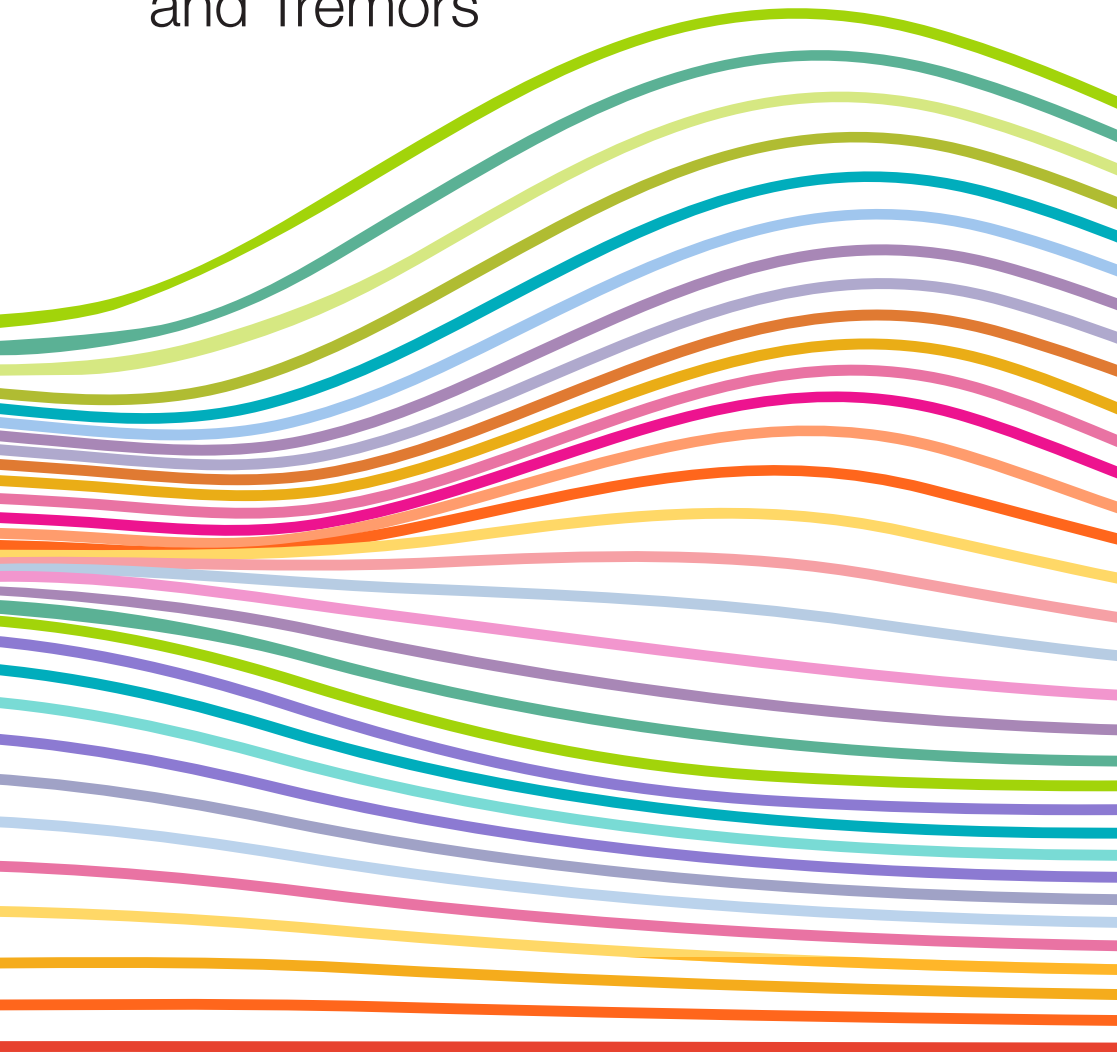

Assimilate

Assessment of Seismic Safety Integrated with Machine Learning and Tremors

risco
universidade de aveiro
risks and sustainability in construction

U.PORTO
FEUP FACULDADE DE ENGENHARIA
UNIVERSIDADE DO PORTO

fct
Fundação para a Ciência e a Tecnologia

FUNDAÇÃO FERNANDO PESSOA

REPÚBLICA PORTUGUESA

Título
Assimilate
Assessment of Seismic Safety Integrated
with Machine Learning and Tremors

Coordenação
Universidade de Aveiro

Parceiros
Faculdade de Engenharia da Universidade do Porto
Universidade Fernando Pessoa

Autores
Vitor Silva
Romeu Vicente
Amir Taherian
Holger Lovon
Feliz Gouveia
Humberto Varum
José Melo
Reihane Panah
Xavier Romão
Catarina Costa

Este trabalho foi financiado pela Fundação para Ciência e Tecnologia no âmbito do projecto ASSIMILATE Assessment of Seismic Safety Integrated with Machine Learning and Tremors PTDC/ECI-EGC/7244/2020.

Earthquake risk assessment is a fundamental step towards disaster risk management. Recent technologies such as low-cost sensors or the advancements in machine learning algorithms have the potential to revolutionize the manner in which earthquake damage and risk is assessed. In the ASSIMILATE project new sensing technology was combined with advanced machine learning algorithms and numerical models to develop a framework for vulnerability and damage assessment. The methods and models produced by this project contributed to the mitigation of several limitations in the current practice regarding vulnerability assessment and rapid loss estimation, and resulted in the installation of 10 sensors in the country that are currently measuring ground motions and building vibrations.

Index

CHAPTER I

01.
Introduction

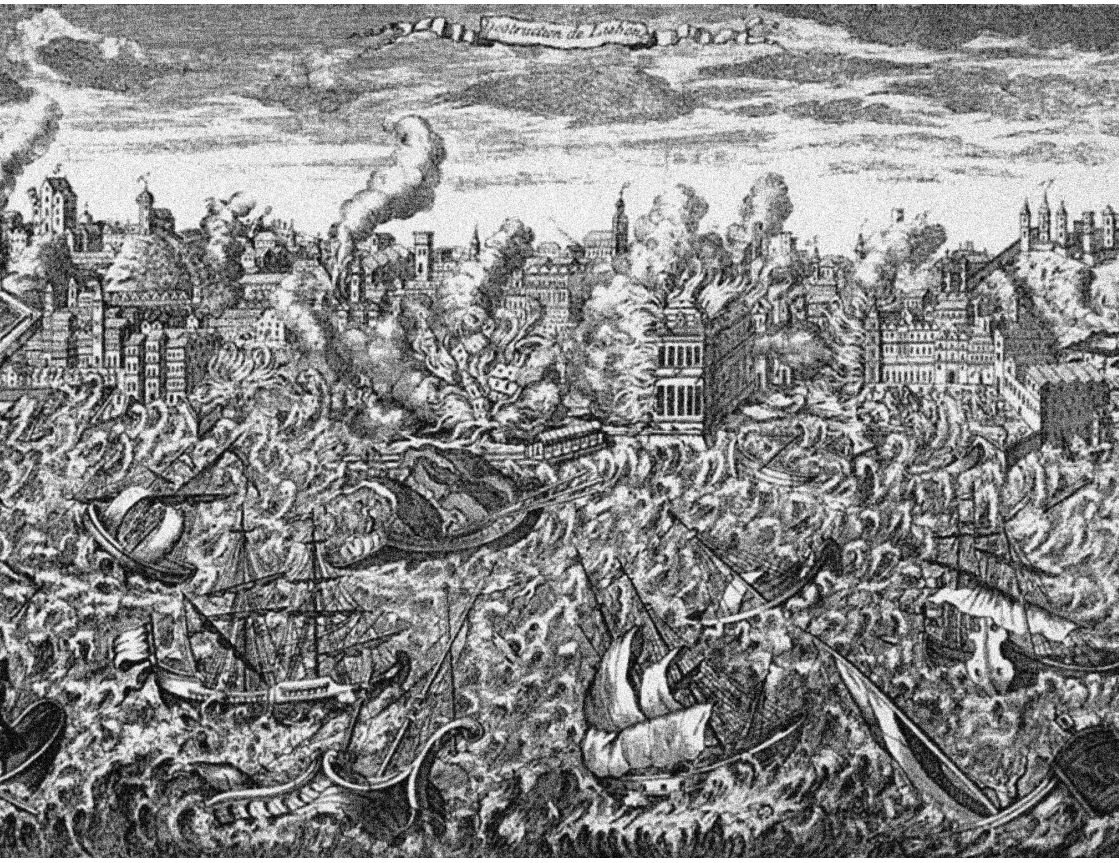
Destruction de Lisbonne

Introduction

Seismic vulnerability and risk assessment are essential steps to better understand, and eventually mitigate, the impact from earthquakes. Prior to the occurrence of destructive earthquakes, risk assessment can support decision makers in the development of retrofitting interventions, or in seeking insurance coverage. An inaccurate assessment of the risk might lead to an overestimation of the level of safety, discouraging houseowners to take measures to reduce their risk. After the occurrence of an earthquake, it is critical to rapidly assess the potential impact and distribute the available resources effectively. Emergency rescue reports from past earthquakes indicate that 95% of the successful rescues of people trapped under debris occur within the first 48 hours, which emphasizes the need to rapidly identify areas in need of support. The assessment of earthquake risk and the rapid estimation of damage are challenging tasks affected by large uncertainties. It is thus important to explore new technologies and tools to improve the process of assessing the seismic safety of buildings before and after the occurrence of destructive events.

Recently developed low-cost sensors to measure vibrations and open-source artificial intelligence tools have the potential to revolutionize the manner in which earthquake damage and risk is assessed. These devices have the capability to transfer data in real--time, and measure ambient vibrations at the top of buildings or ground motion at the foundation. These vibrations can be used to

calibrate vulnerability models or to estimate the expected damage after the occurrence of destructive events. Despite the usefulness of such technology, there are still challenges in its employment, which currently prevents its effective application. While the measurement of the dynamic properties of a single building to calibrate a numerical model is commonly performed, their integration on vulnerability modelling for building portfolios has not been explored. Consequently, monitoring data is rarely used for the calibration of vulnerability functions for large building portfolios, thus hampering their exploitation in risk modelling, which could improve considerably the quality of loss models. On the post-event side, data regarding the structural response of buildings is not used on an operational basis, and seismic networks are sparse and limited to a few stations per urban centre. For example, mainland Portugal has less than 50 recording stations in its territory, which might prevents the accurate estimation of ground shaking in some populated areas.

The reasons for the inability to integrate monitoring data in portfolio risk analyses or to accurately estimate structural damage are due to the high costs involved in the installment and maintenance of sensors, as well as lack of knowledge regarding the integration of large complex datasets (big data) in vulnerability and loss assessment. The former issue is now being overcome with the availability of low-cost sensors, while the latter challenge is being revolutionized by artificial intelligence (and in particular machine learning) technology that can process large amounts of data to predict complex outcomes. Some of the open-source tools allow researchers to integrate machine learning into their computational frameworks. In vulnerability modelling and damage assessment, machine learning enables the incorporation of a wide range of data regarding the dynamic properties of structures to better calibrate numerical models, as well as the exploration of a multitude of structural response and ground motion parameters to better estimate shaking and damage in near-real time.

In the ASSIMILATE project we combined low-cost devices with machine learning technology and numerical models to develop a framework for vulnerability and damage assessment. To this end, a database of dynamic properties of Portuguese buildings was created, and low-cost sensors were installed in several buildings to collect additional data, which was used to calibrate numerical models. Moreover, data recorded from past events was explored to expand the framework to the estimation of damage and losses using monitoring data captured in near-real time. The consortium involved in this project included partners with decades of experience in seismic monitoring, vulnerability modeling and processing of large datasets using machine learning. The methods and models produced by this project contributed to the mitigation of several limitations in the current practice regarding vulnerability assessment and rapid loss estimation. The main contributions of this project include:

1) Compilation of a database of dynamic properties for Portuguese buildings;
2) Development of a new national exposure model for earthquake scenarios and probabilistic seismic risk assessment;
3) Development of vulnerability functions for reinforced concrete structures based on period elongation;
4) New sets of fragility and vulnerability functions for the (granite and limestone) unreinforced masonry building stock;
5) A new ground motion model for mainland Portugal using stochastic simulations that can be combined with low-cost sensors;
6) A demonstration of the benefits of seismic monitoring using dense seismic networks in the district of Lisbon;
7) A design of a rapid loss assessment system for Portugal, and integration of conditioning modules on an open-source tool;
8) An assessment of seismic risk for Portugal covering give risk metrics, which can be used to identify areas where low cost sensors should be installed;
9) Installation of 10 new seismic monitoring sensors in Portugal, which can be used for rapid loss assessment.

This project had several stakeholders such as the Portuguese Civil Protection Authority, the Portuguese Institute of the Sea and Atmosphere (which monitors seismic activity), the National Laboratory of Civil Engineering, the Global Earthquake Model Foundation and SafeHub. It also contributed to the goals of the international agendas of the Sendai Framework and the United Nations 17 Sustainable Development Goals, which ask specifically to better understand risk and reduce the impact of natural hazards.

CHAPTER II

02.

Exposure Model for the Residential Building Stock in in Portugal

Exposure Model for the Residential Building Stock in in Portugal

Exposure models include detailed information about the spatial distribution of the built environment, namely its geographical location, number of buildings, structural properties, replacement costs, and number of occupants. The exposure models for Portugal used in previous risk studies were developed using information from the 2011 national housing census (Silva et al., 2014; Sousa and Costa 2016), and neglected the commercial and industrial building stock. With the release of new data collected in the context of the 2021 national housing census (https://censos.ine.pt/), it is now important to update the existing model and understand how this new information can impact the risk estimates. Moreover, within the scope of the European H2020 SERA project, an exposure model for the commercial and industrial building stock covering Portugal was developed (Crowley et al. 2020). In this chapter, we describe how the new exposure model for the residential building stock was developed, and we summarize the main features of the commercial and industrial building stock released as part of the SERA project. This model was fundamental for the impact analysis performed within the scope of ASSIMILATE.

Residential building stock

The latest housing census for Portugal captures detailed information about the residential building stock, including the number of buildings at the statistical section (i.e., an administrative division defined specifically for the national census), disaggregated by the number of storeys and year of construction. In contrast with the previous 2011 census data, this newer assessment did not include the type of construction of each building (i.e., reinforced concrete, masonry with a slab, masonry walls without slab, adobe walls or loose stone masonry, and other), which is fundamental to categorize each building into a vulnerability class. For this reason, the information about the number of buildings within each construction type from 2011 was used in the development of the new model. To adjust these values to the current number of buildings, we calculated the difference in the number of buildings between 2011 and 2021. Then, for each parish (freguesia), it was assumed that if this difference is negative (i.e., the number of buildings in 2021 is lower than in 2011), the buildings that were demolished were either masonry or older buildings, and therefore these were excluded from the model. On the other hand, when there was an increase in the number of buildings, we assumed that the new buildings were constructed using reinforced concrete.

The housing census of 2021 reports approximately 3.5 million residential buildings, comprising 6 million dwellings. Considering the attributes available for each building (type of construction, year of construction and number of storeys), the building portfolio was divided into different building classes following the GEM building taxonomy (Silva et al. 2022). According to the type of construction, the buildings were categorized into 5 main classes: reinforced concrete (CR) buildings, brick/stone masonry (with wooden floors (MUR+FW), or with concrete floors (MUR+FC), adobe masonry buildings (MUR+ADO), and other/unknown typologies (UNK). As shown in Fig. 1, the majority of the building stock is made of

reinforced concrete (53.7%), housing around 63% of the population.

The year of construction allows understanding the level of seismic design in place when the buildings were constructed. By comparing the construction year classes available in national housing census with the evolution of seismic codes in Portugal (e.g. Silva et al. 2014), four design levels were defined: no-code (CDN) refers to buildings built before 1960, low code (CDL) from 1961 until 1980, moderate code (CDM) from 1981 until 2010, and high code (CDH) refers to structures built after 2011. It is relevant to note that around 36% of the building stock has been built before the introduction of the 1983 design code (RSA 1983). Fig. 1 shows the distribution of buildings for each construction typology, according to the construction period and number of storeys. We note that even if an adobe or unreinforced masonry building was built recently (and would thus fall under the CDM or CDH category), the building is still assumed to have limited seismic capacity, as dictated by the vulnerability model described in the following section.

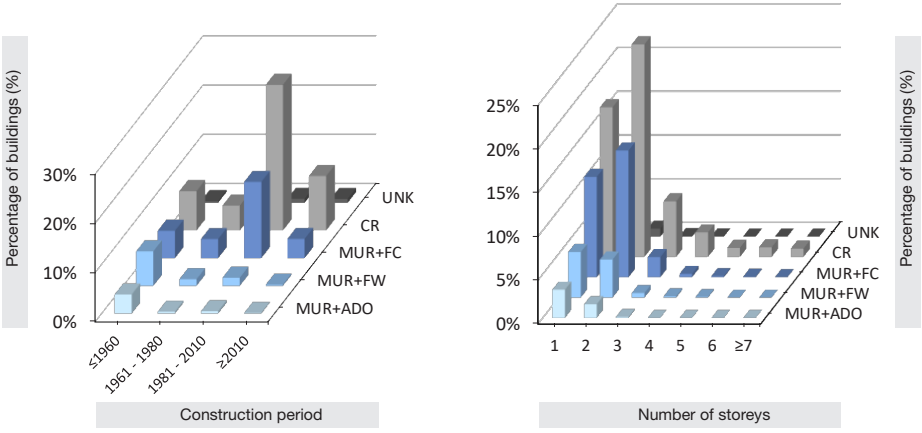

Figure 1. Distribution of buildings according to type of construction, construction period, and number of storeys

For the estimation of economic losses, it was necessary to establish a replacement value for each building, which corresponds to the cost required to build a structure with the same characteristics and area, based on current construction costs. To calculate the total replacement cost of each building, we multiplied the average construction cost per square meter by the total area of the building. The area of each building was estimated considering the average number of dwellings per building and the average area per dwelling. Although the census data does not have disaggregated data on the number of dwellings per building type, it provides the distribution of the number of dwellings according to the building height. This allows us to calculate the average number of dwellings for buildings with a specific number of storeys. As shown in Table 1, buildings with 3 storeys, for example, have on average 2.08 dwellings.

Table 1. Average number of dwellings per building per number of storeys

1 storey	2 storeys	3 storeys	4 storeys	5 storeys	6 storeys	≥7 storeys
1.04	1.15	2.08	6.55	9.78	11.83	15.41

Regarding the average area per dwelling, it is important to distinguish separated houses from apartment buildings, as the latter tends to have smaller areas. The National Statistical Office (INE) provides information concerning the area per dwelling for the seven areas defined by the Coordinating Committee for Regional Development (CCRD) in Portugal, with an average value for the country of 101 m^2. We assumed that this is a reasonable value for dwellings in apartment buildings. For separated houses, we reviewed hundreds of entries in real estate web portals to define a reasonable dwelling area. From this review, and based on the data from INE, we assumed that buildings with 1 storey or 2 storeys are houses with an average area of 150 m^2 and 120 m^2 per dwelling, respectively, while buildings with 3 storeys or more are apartment buildings with an average area per dwelling of 100 m^2.

The construction costs per square meter have important variations throughout the country, depending on the building location. The housing construction price in 2022, calculated according to the traditionally accepted method by the majority of insurers operating in Portugal, are divided in 3 zones. Zone I includes the district capitals, other major cities and the islands (830.03 €/m^2), zone II includes counties located in urban areas (725.56 €/m2), and Zone III refers to counties located in rural areas (657.35 €/m^2).

To estimate the number of occupants in each building, we multiplied the average number of occupants per dwelling by the number of dwellings in each building. The average number of occupants per dwelling was calculated by dividing the total population (10.3 million) by the total number of dwellings (6.0 million), resulting in 1.72 occupants per dwelling.

Commercial and Industrial building stock

Information regarding the industrial and commercial building stock is far less detailed than the residential counterpart, both in terms of spatial resolution and construction attributes. This is a trend that is common to most countries (Yepes et al. 2023), leaving exposure analysts with no alternative but to use simplified methodologies. In this project, commercial buildings include offices, wholesale, retail (trade), and hotels, while the industrial facilities cover manufacturing, mining, quarrying, and construction activities. As previously mentioned, we adopted the commercial and industrial building stock for Portugal developed within the scope of the H2020 European SERA project. We summarize herein the methodologies that were followed for the development of these models, and additional details regarding the derivation procedure and assumptions can be found in Crowley et al. (2020).

For the development of the commercial building stock, socio-economic data was collected from the National Institute of Statistics (INE) regarding the number of (commercial) businesses. Assuming that each business requires a building or facility, this step led to the number of buildings at the second administrative level. Then, a mapping scheme was applied to each type of commercial activity to attribute a building class to each asset. The cost of each asset was determined by assuming an average area and a construction cost, which again is dependent on the location of the building. We note that some commercial activities (in particular wholesale and retail), are located on the ground floor of residential buildings. These buildings of mixed use are identified within the national housing census (approximately 10% of the residential buildings in Portugal). This information was used to reduce the number of commercial buildings, to avoid double counting the construction area of this type of activity.

The development of the industrial building stock followed a different approach, as originally described in Sousa et al. (2017). For this type of buildings, an European land cover dataset (CORINE 2006) was used to identify the areas in Portugal where industrial buildings might exist, and the number of facilities were identified using data from OpenStreeetMap (REF). A statistical process was applied to understand which industrial areas had all buildings identified (within OpenStreetMap), and which areas were incomplete, and thus required the application of an extrapolation procedure based on the estimates derived for the complete areas. For the specific case of Portugal, this procedure was validated against detailed cadastral data regarding industrial buildings from 18 districts (Araujo et al. 2015). The commercial and industrial exposure models are available in the EFEHR exposure repository (https://gitlab.seismo.ethz.ch/efehr/esrm20_exposure), along with all of the assumptions concerning areas, costs, and mapping schemes.

Appraisal of the exposure model for Portugal

Residential buildings represent most of the exposure model for Portugal, accounting for 92.4% of the number of buildings, while commercial and industrial building represent 4.8% and 2.8%, respectively. In terms of replacement cost, residential buildings represent a lower fraction (78.9%) due to the high costs of the contents in commercial and industrial buildings. These distributions are depicted in Fig. 2.

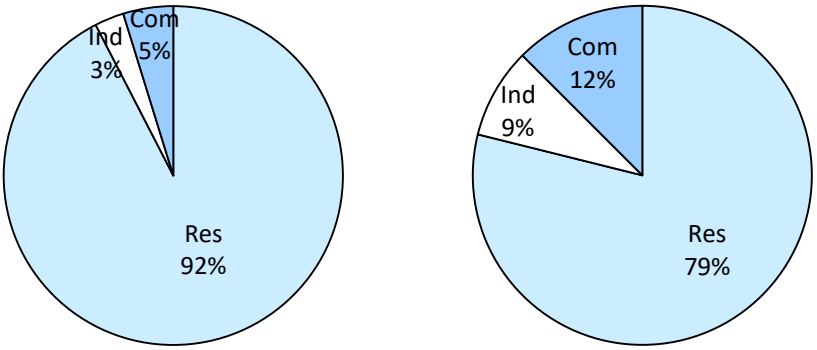

Figure 2. Distribution of the number of buildings (left) and replacement cost (right) by occupancy

Fig. 3 summarizes some of the main indicators of exposure model aggregated at the district level, while Fig. 4 and 5 present the economic value and number of buildings at the smallest available administrative division (i.e., freguesia). These results indicate that more than 50% of the economic value of the building stock is concentrated only in four districts (Lisbon, Porto, Setubal, and Braga), while the number of buildings is more uniformly distributed, with half of the building stock located in the top 6 districts. It is interesting to note the variation in the percentage of buildings with insufficient seismic provisions (from 42% in Madeira to 79% in Portalegre and Beja). It is also important to highlight that only 12% of the total number of buildings follow the most recent seismic regulation. These are important findings, as they allow identifying concentrations of exposure with an expected poor seismic performance, and thus where additional risk analyses should be performed.

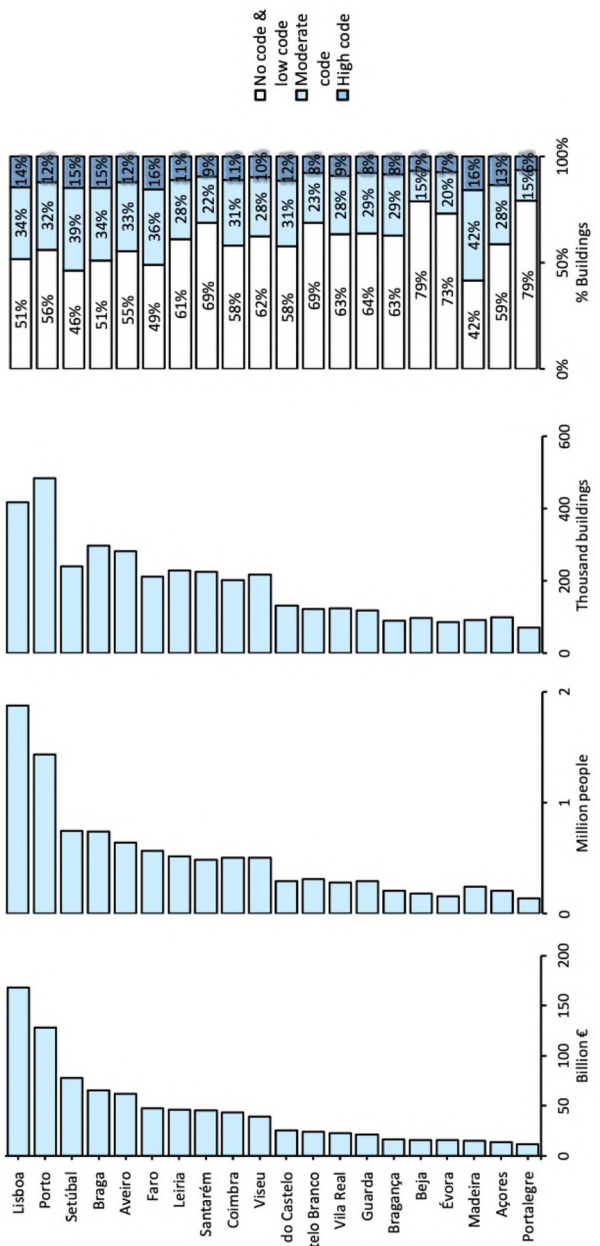

Figure 3. Exposure indicators of the Portuguese building stock per district

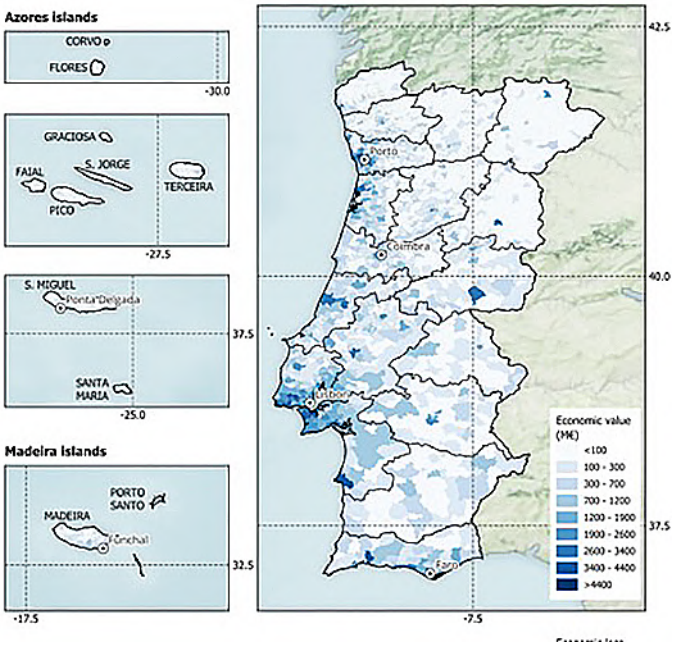

Figure 4. Economic value at the smallest available administrative division (i.e., *freguesia*)

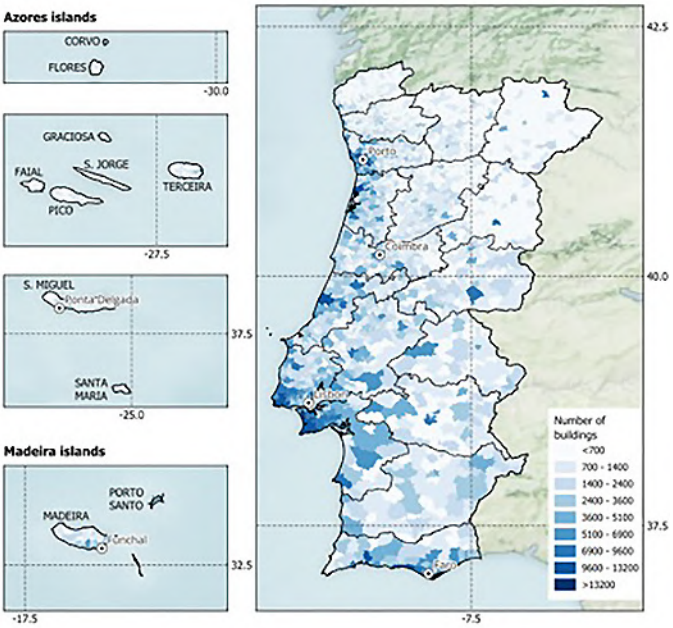

Figure 5. Number of buildings at the smallest available administrative division (i.e., *freguesia*)

CHAPTER III

03.

Exploring Modal Parameters for Vulnerability Analysis

Exploring Modal Parameters for Vulnerability Analysis

During the past two decades, a significant number of studies have been carried out in the field of Non-destructive Damage Evaluation (NDE) methods using the changes in the dynamic response of a structure. The NDE methods can be classified into different levels, according to the complexity of the information available for the analysis. Each level of damage identification requires a gradually increasing amount of data and more complex algorithms. Consequently, their set-up and effectiveness often require increasing costs, with higher error probability, however, rapid damage assessment is the practical issue in assessing the damage of structures for making decisions about their functionality Gallipoli et al. (2020). Measuring the dynamic parameters of structures and finding the relation of its changes with different levels of damage can be a useful and cost-effective way to rapidly assess potential damages due to earthquakes. Therefore, vulnerability assessment based on the result of monitoring structural modal parameters variation can be a useful method with a high level of accuracy.

One of the main modal parameters of a structure is the period of vibration that is mainly influenced by its total mass and stiffness. During an earthquake, damage affects both structural and non-structural elements, leading to a decrease in their stiffness. This phenomenon is known as "period elongation," and essentially, the

more severe the damage, the more significant the increase in the period compared to the undamaged state. The extent of period elongation is a helpful indicator of the building's damage state and vulnerability assessment: higher elongation implies more significant damage. The extent of damage to these components, commonly termed as a Damage Limit State (DLS), can be assessed either through visual inspection or by using numerical analyses that correlate the exceeding of a certain Engineering Demand Parameter (EDP) threshold with the attainment of a specific DLS for a specific earthquake scenario.

In this project, we conducted numerical time history and pushover analyses of reinforced concrete buildings. The pushover analysis was used to determine the thresholds for a set of DLS of infilled RC structures. The main objective of this part of ASSIMILATE was to establish a relationship between period elongation and structural damage, which can be analytically measured using finite elements methods. The aim is to determine whether the building's period elongation can be a reliable indicator for assessing its vulnerabilityand loss estimation after an earthquake.

Development vulnerability functions based on period elongation

Five example buildings located in Portugal were considered for this study: 4-storey and 3-storey RC buildings with infill walls with different seismic design coefficients (beta equal to i.e., 20, 10, 5 and 0 %). Information about the geometrical and material properties of these archetypes can be found in Table 1 and Figure 1.

Table 1. General description of buildings information

No of building	Length X (m)	Length Y (m)	Fcd (MPa)	Fsyd (MPa)	ax (m)	ay (m)	astair (m)	beta	Number of storey
1	25,75	12	7	10,5	5,65	4	3.16	0	3
2	25,75	12	7	10,5	5,65	4	3.16	5	3
3	25,75	12	7	10,5	5,65	4	3.16	10	3
4	25,75	12	7	10,5	5,65	4	3.16	10	4
5	25,75	12	7	10,5	5,65	4	3.16	20	4

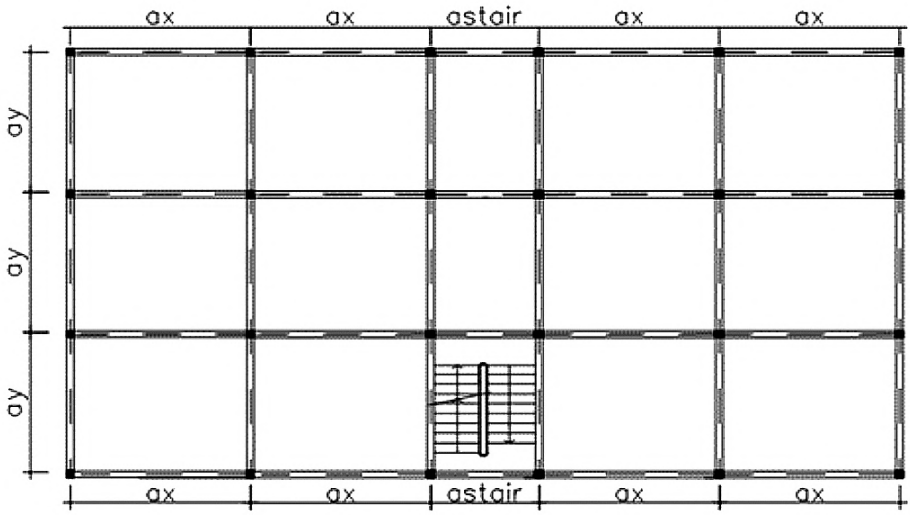

Figure 1. Geometry of case-study building

The non-linear response of buildings was modeled using the OpenSees software by adopting a lumped-plasticity approach. Structural vulnerability assessment is characterized by significant uncertainty due to ground motion, as noted by Shome and Cornell (1999). Therefore, particular attention was paid to the selection of ground motion records. The conditional spectrum method (CSM) proposed by Baker (2011) was utilized to select 180 ground motion records used in the numerical analysis. The response spectra of the chosen records are displayed in Figure 2.

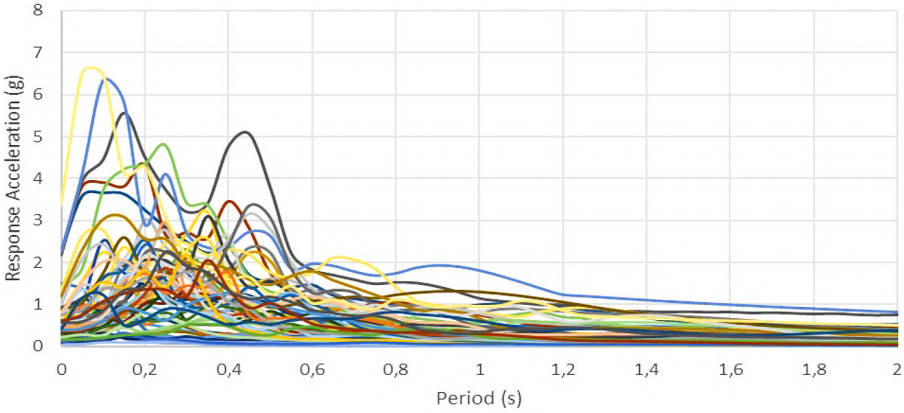

Figure 2. Elastic response spectra of the selected ground motion records conditional to T=0.3s

The seismic loads were applied to the structure's foundation, perpendicular to its length. The structural damage was categorized into four damage states: slight, moderate, extensive, and complete damage. The threshold values for each damage state were determined based on the anticipated yield and ultimate displacements derived from the pushover analysis. The ultimate displacement is considered as the point with 20% reduction of base shear. Finally, for each capacity curve, a quadrilinear curve was fitted.

Traditionally, vulnerability functions were developed from the convolution between fragility models and discrete damage-to-loss models (see example in Table 2). However, to preserve the variability in the loss estimates, the methodology proposed by Silva (2019) which correlates the expected Loss Ratio (LR) at different damage states directly with an EDP was adopted. Combining the damage thresholds computed from the capacity curve with the damage-to--loss model in Table 2 produced a discrete relationship between the structural performance and expected loss (depicted in Figure 4 as vertical bars).

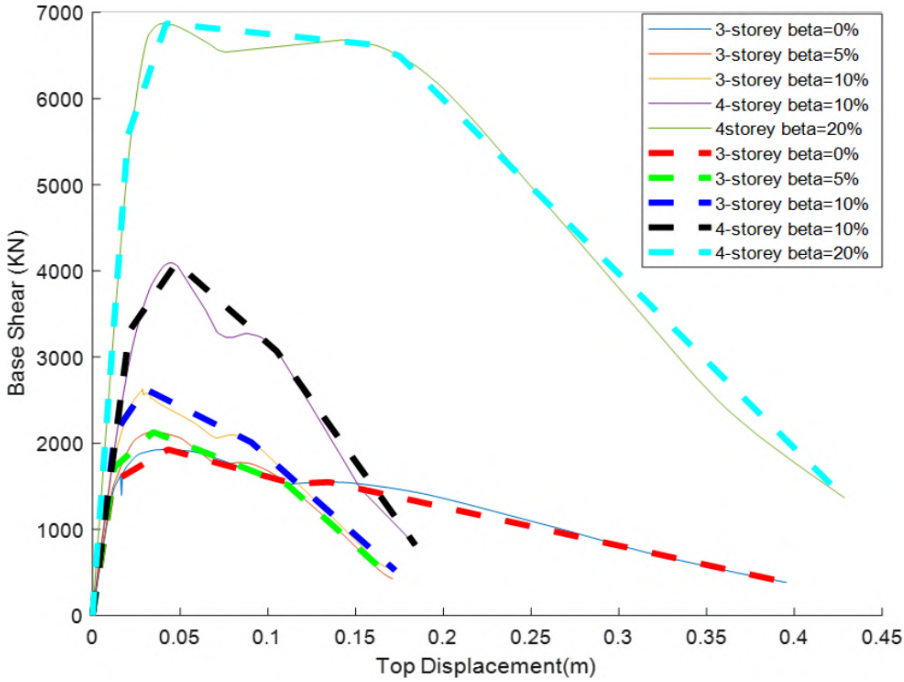

Figure 3. Capacity curves for the case study buildings

Table 2. Discrete damage-to loss model

Damage State	Loss Ratio (LR) (%)
Slight Damage (DS1)	5
Moderate Damage (DS2)	20
Extensive Damage (DS3)	60
Complete Damage (DS4)	100

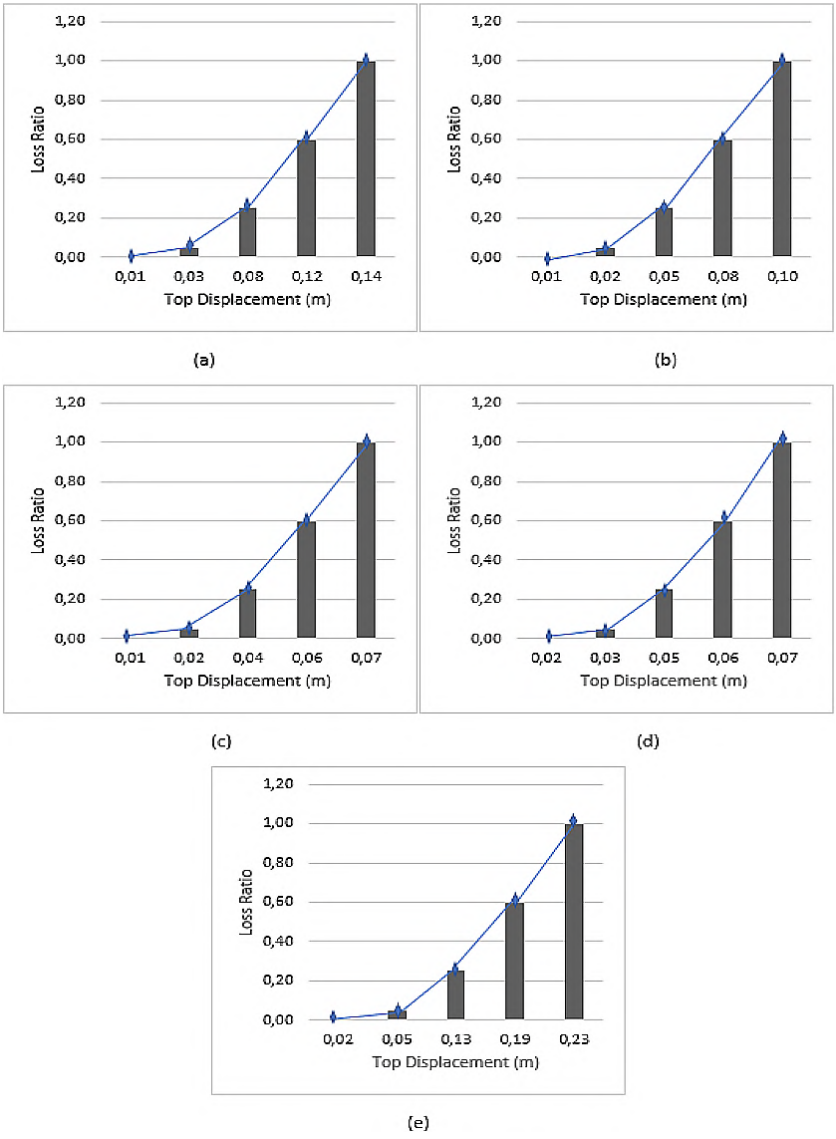

Figure 4. Relation between the LR (Loss Ratio) and Sd (Sdu and Sdy) for each building; a) 3-story with beta=0%; b)3-story with beta=5%; c)3-story with beta=10%; d)4-story with beta=10%; e)4-story with beta=20%

The Open Sees software was chosen due to its capability to perform Eigenvalue analysis to determine the period of vibration of the structure at any step. We estimated the period elongation by comparing the original period (T1) with the period of vibration at the final time step (T2). After the estimation of the period elongation and the expected loss ratio for each ground motion record, a new vulnerability function was derived, as presented in Figure 5 using the period elongation as the independent variable.

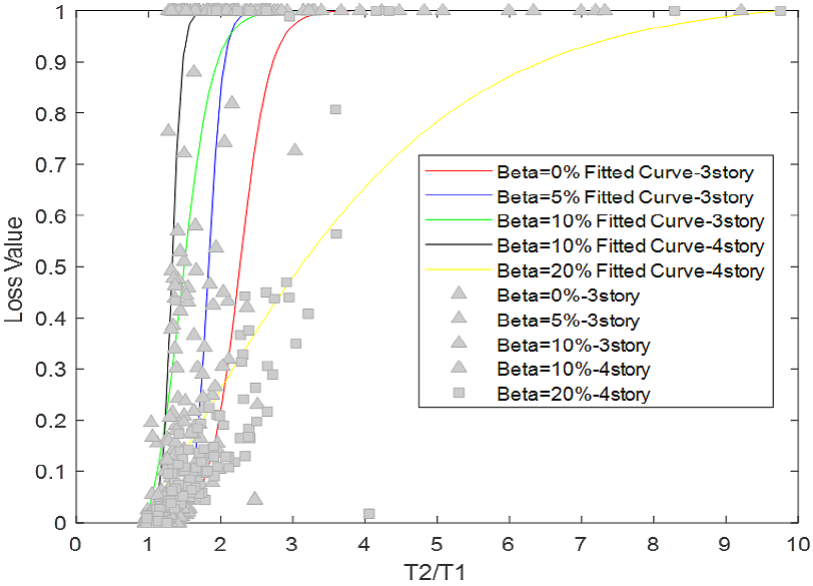

Figure 5. Period elongation versus loss ratio

Based on the vulnerability results, it is possible to observe that the loss ratio increased with different values of period elongation depending on the seismic coefficient that the structure was designed for. Figure 5 revealed that for structures that are designed for seismic coefficient equal to 20%, the maximum loss ratio occurred at a higher period elongation. Furthermore, the maximum loss value is reached after the elongated period reaches 2 for the structure not designed for seismic loadings.

Another important part of this analysis was the verification of the results based on the previous studies by considering some variables such as difference in infill panels, materials, structural seismic design coefficient and other parameters to approximately verify our analysis against experimental results. This verification also produces a quantification approach for rapid damage assessment of structures. One of the most relevant measurements on this topic was produced by Vidal et al (). The Figure 6 shows the relation between maximum, minimum and average period elongation versus grades of damage. We concluded that the average variations of T >10 % indicate the occurrence of damage in buildings. For average variations of T >55 %, the buildings were completely damaged. The collapse of structures occurred at maximum period elongation equal to 150% which is similar to the conclusion by Calvi et at. (2006). These results are also in line with the results of Vidal et al. (2014) where 23 reinforced concrete buildings were analyzed before and after the Lorca earthquake.

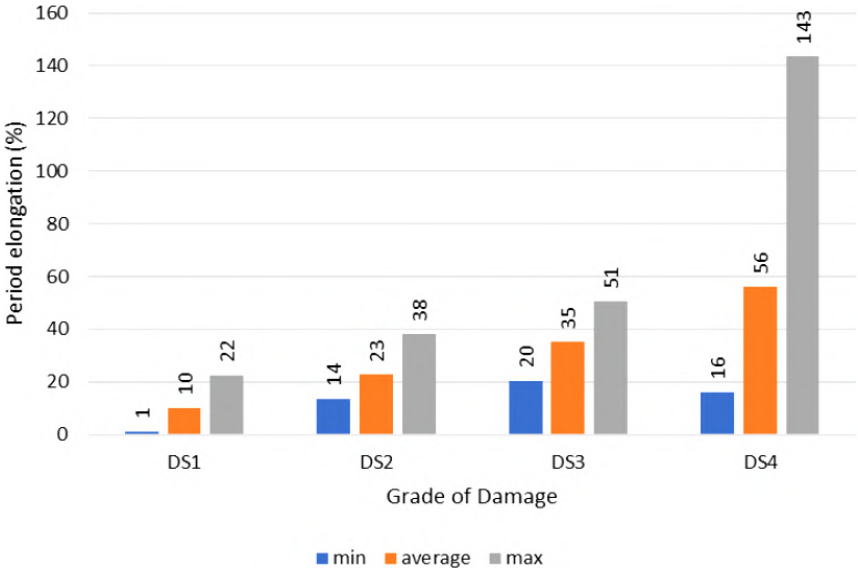

Figure 6. Period elongation versus degree of damage

These functions can be combined directly with the low-cost sensors that were used within the scope of the ASSIMILATE project. Once a sensor is installed, it can measure both the period of the structure before any damage occurs, and then again after the occurrence of a seismic event. If a period elongation is detected, the vulnerability functions presented herein can be used to determine the most likely level of damage or loss. This approach is superior to conventional methodologies that use an intensity measure (e.g., peak ground acceleration or spectral acceleration), as period elongation has a direct correlation with loss of structural stiffness due to damage initiation.

CHAPTER IV

04.

Vulnerability Assessment of Unreinforced Masonry

Vulnerability Assessment of Unreinforced Masonry

The assessment of the impact of earthquakes on livelihoods requires models that can directly relate the expected number of building occupants to different injury levels conditional on an intensity measure (IM) (i.e., fragility functions). However, the vast majority of the existing fragility studies focused on the assessment of structural damage (Yepes et al. 2016) or economic losses (e.g., collapse risk in RC buildings, damage in masonry buildings). This lack of fragility or vulnerability functions to evaluate the human impact hinders the availability, accuracy, and reliability of fatality modelling studies. This aspect was particularly important within the scope of the ASSIMILATE project, given that one of the goals was to design a rapid loss assessment system to assist the population in case of a destructive event.

Past efforts focusing on assessing human losses have followed two main approaches: 1) empirical functions based on databases of human losses, and 2) hybrid approaches that combine fragility functions with empirical (or expert judgement) fatality rates. The former approach consists of developing statistical models that relate fatality rates directly with a magnitude or an IM (e.g., Moment magnitude - Mw or Modified Mercalli Intensity - MMI). In the hybrid approach, the assessment of human losses or injured is performed through the application of ratios that convert the probability of complete

structural damage (i.e. a level of damage beyond the possibility of repair) into a probability of collapse, which is then further converted into a probability of fatality (or injured) based on empirical ratios (e.g., Spence 2007, FEMA 2018). This approach has the advantage of allowing users to take advantage of existing fragility functions originally derived for structural damage (e.g., Ceferino et al. 2018, Maio et al. 2020). However, the employment of such rates might lead to unrealistic fatality rates, particularly for seismic events where extreme ground shaking is generated. This procedure is illustrated in Figure 1. In this example, an existing fragility function for complete damage (i.e., herein termed as DS4 following the damage scale from Martins and Silva 2020) is converted into a probability of collapse using a collapse probability conditional on complete damage (P[col|DS4]), and then converted into a probability of fatality using a fatality rate conditional on structural collapse (P[F|col]).

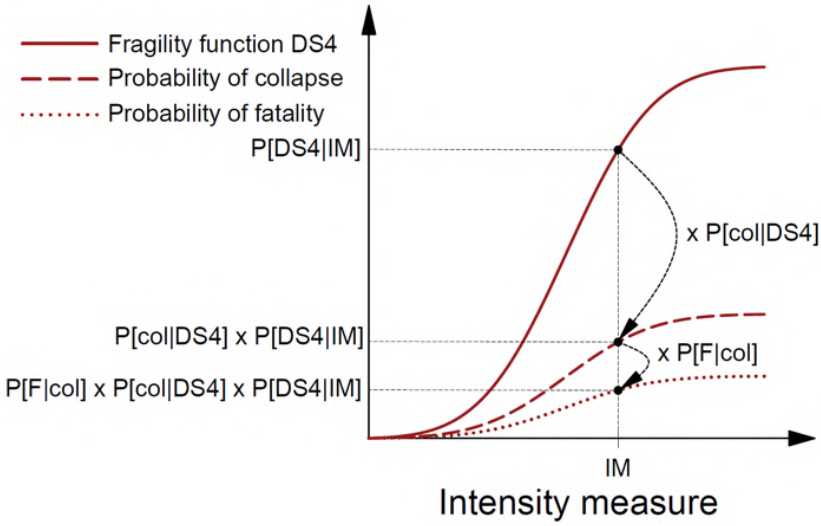

Figure 1. Procedure to derive a vulnerability function in terms of fatality rates, starting from an existing fragility function for structural damage of a 2-storey unreinforced masonry building

This approach for the derivation of vulnerability functions for the assessment of fatalities can lead to a rapid saturation of the fatality rates, even for extremely high IM, potentially underestimating the expected losses for strong seismic events. For the example presented in Figure 1, even when the probability of complete damage reaches 100%, the probability of fatality is 1.52%. In contrast, the average fatality rates for the collapsed buildings in the 2019 M6.4 Durres (Albania) and 2020 M6.7 Elazig (Turkey) earthquakes were approximately 45% (So and Pomonis 2012), twice the value proposed by HAZUS. One of the limitations of this approach is the reliance on traditional damage states and conventional engineering demand parameters (EDPs – e.g., maximum inter-story drift ratio), which cover a wide range of damage levels (i.e., from damaged beyond repair to full collapse), which will obviously influence the likelihood of injuries and fatalities (e.g., Crowley et al. 2017; Abeling and Ingham 2020).

It is thus important to consider alternative approaches to measure the level of damage in buildings exposed to strong ground shaking. So (2016) did a thorough review of damage and fatality data from 25 fatal earthquakes between 1968 and 2011 and established a correlation between typical volume loss and fatality rates for several building classes. Abeling and Ingham (2020) used survey data from the M7.1 2010 Darfield and M6.2 2011 Christchurch earthquakes to evaluate the correlation between volume loss and fatality ratios. In these examples, a strong correlation between volume loss and fatality rates was observed. In ASSIMILATE, a framework was developed to derive fatality vulnerability functions that combine the results of numerical simulations with empirical fatality rates, such as the ones proposed by the studies presented previously. Recent numerical approaches and laboratory tests were leveraged to develop 3D models representative of masonry structures. Archetypes were selected using statistical models representing the geometric and material properties of limestone and granite buildings from Portugal (Lovon et al. 2022).This structural typology is particularly prevalent in Portugal (accounting approximately for 50% of the residential building stock). Nonlinear time-history analyses were performed

using a suite of ground motion records, and the results were used to estimate the volume loss for each analysis. Then, this metric was converted into fatality rates using an existing empirical model. These functions and the exposure model presented in Chapter 2 were used for the evaluation of the benefits of seismic monitoring in the country using low-cost sensors.

Characterization of the masonry building stock

The vulnerability methodology presented in this study has been applied to the Portuguese masonry building stock, which is the most vulnerable fraction of the national building stock, representing almost 50% of the number of buildings. Figure 2a illustrates the date of construction combined with the number of storeys of masonry buildings in Portugal. The construction of masonry buildings has been decreasing in recent decades, but it is still used throughout the country, including in regions with a relatively high seismic hazard (i.e., PGA $\geq$ 0.25g for the 475-year return period on soil conditions). Figure 2b presents the annual growth rate of this type of construction in the last 100 years according to the level of seismic hazard. The seismic input was calculated using the model from Vilanova and Fonseca (2007).

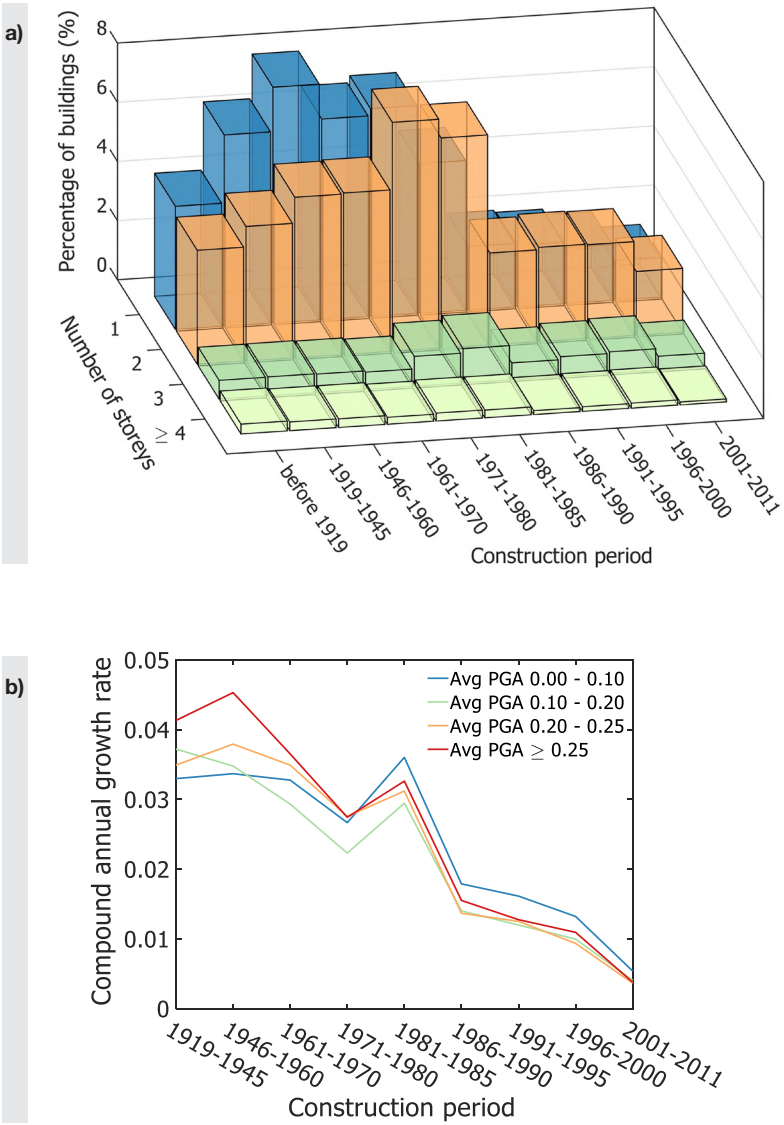

Figure 2. Distribution of masonry buildings per construction period and number of storeys, and Compound annual growth rate of masonry construction per period at different levels of seismic hazards for a 475-year return period on soil conditions

Limestone and granite are the most common types of stones employed for masonry construction in Portugal's central and northern regions, respectively. Lime-sand mortar is usually employed for bed joints, yet a minor proportion of buildings, mainly granite masonry buildings, present dry joints as this type of joint is associated with heritage architecture. Inter-storey systems are made either of timber or reinforced concrete in similar proportions, while the roof is typically made of timber and ceramic tiles. Most common foundations for this building type consist of an enlargement of the masonry walls at the base using materials with poorer quality and arrangement.

Lovon et al. (2021) investigated the geometric features of limestone and granite buildings based on a database of 200 existing structures. From this review, statistical models were developed for a set of 10 geometric features, as presented in Table 1. The mechanical properties of this type of construction have been the subject of several past studies, which indicate a large variability for most of the parameters. This uncertainty can be attributed to the wide diversity of masonry assemblies, differences in the unit size, type of mortar, irregularities and degradation. Another important source of uncertainty is the type of test performed to obtain those properties, ranging from static, cyclic, time-history, in-situ, laboratory, destructive, semi-destructive and non-destructive. Conscientious of this variability, the mechanical properties adopted in this work are summarized in Table 1.

Table 1. Geometric and mechanical properties of limestone and granite masonry buildings

Element	Description	Unit	Limestone	Granite
Geometric properties	Ground floor height	m	N(2.98,0.46)	N(3.60,0.39)
	Upper stories height	m	N(2.90,0.31)	N(3.30,0.39)
	Length X-direction	m	Log(6.7,2.70)	Log(6.20,0.94)
	Length Y-direction	m	N(8.20,2.10)	N(17.0,3.90)
	Wall thickness (≤3 stories)	m	Wei(0.66,0.07)	Wei(0.54,0.11)
	Wall thickness (>3 stories)	m	Log(0.69,0.08)	N(0.61,0.11)
	Average wall thickness reduction	-	Γ(0.15,0.09)	Γ(0.16,0.08)
	Opening ratio (ground)	-	Beta(0.46,0.14)	Beta(0.55,0.13)
	Opening ratio (upper stories)	-	Beta(0.27,0.05)	Beta(0.43,0.10)
	Non-structural walls density	-	Γ(0.026,0.01)	Γ(0.026,0.10)
Bricks (solid elements)	Elasticity modulus	GPa	0.76	0.93
	Poison ratio	-	0.30	
	Static coefficient of friction	-	0.80	
	Dynamic coefficient of friction	-	0.60	
	Penalty stiffness factor	-	1.00	
Mortar (cohesive elements)	Normal failure stress	MPa	0.12	0.15
	Shear failure stress	MPa	0.12	0.15
	Normal energy release rate	N/m	30.00	36.00
	Shear energy release rate	N/m	30.00	36.00
	Normal stiffness	GPa	0.76	0.93
	Tangential stiffness	GPa	0.76	0.93
Beams	Timber elasticity modulus	GPa	7.00	
	Design compressive strength	MPa	16.00	

* are the Normal, Lognormal, Weibull, Gamma and Beta distributions, respectively, defined by the mean and standard deviation

Due to the absence of destructive events in the last decades in mainland Portugal, there is a lack of damage data for these building typologies. Thus, the expected damage patterns must be inferred from similar types of construction or experimental campaigns. From the review of the literature, we identified two main failure mechanisms. The first failure type is herein termed as "zero" mechanism, and it is one of the primary causes of building collapse. It consists of the disaggregation of masonry elements due to the poor quality and lack of capacity to resist horizontal forces, as depicted in Figure 3. The second failure type is the out-of-plane mechanism, which consists of the total or partial overturning of a façade. An example of an out-of--plane mechanism is shown in the same figure. Other important damage mechanisms include vertical instability of the walls, bending rupture, corner overturning, and roof pounding (Indirli *et al.* 2013).

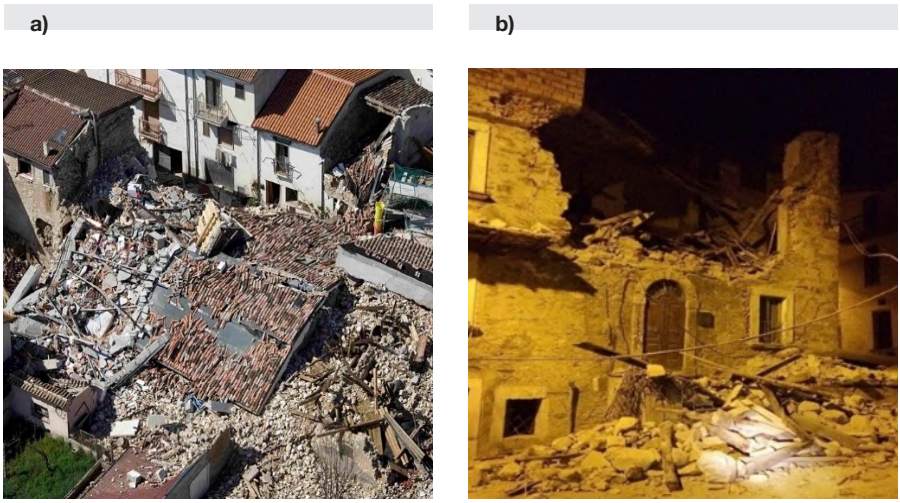

Figure 3. "Zero" collapse mechanism (left) and out-of-plane failure mechanism (right) observed in the Mw 5.9 L'Aquila Earthquake

Framework for fatality vulnerability assessment

With the significant advancements in numerical modeling of masonry buildings, it is possible to explicitly simulate structural collapse. For example, Grant et al. (2021) modeled a 2-storey unreinforced masonry building representative of the Groningen region (Netherlands) and quantified the probability of explicit collapse through nonlinear time-history analysis. This type of analysis allows taking advantage of engineering demand parameters (EDPs) that characterize the level of destruction explicitly. The framework for fatality vulnerability assessment followed in ASSIMILATE starts with the generation of single or multiple 3D building models based on existing geometric and mechanical models (see Table 1). These models are subjected to nonlinear time-history analyses using a set of ground motion records, and an algorithm is used to estimate the volume loss resulting from each analysis.

Numerical modeling

We created 3D numerical models for 1, 2, 3 and 4-storey limestone and granite buildings. Using the sampled openings area, a façade configuration was assigned according to the archetypes depicted in Figure 4. The relation between the opening area and the layout of the façade was established based on the information obtained from the database of existing masonry buildings, as described in Lovon et al. (2021) A single archetype was selected for the vulnerability analysis for the remaining building classes due to the high computational cost. We adopted the archetypes whose geometrical properties were closest to the average geometric features found in the previous studies.

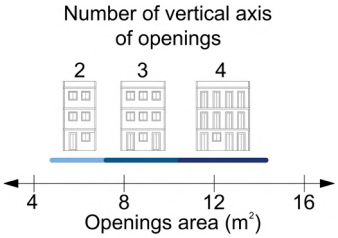

Figure 4. Façades archetypes and openings area

The strategy adopted herein for the numerical modeling of these structures consists in discretizing each building into a set of homogeneous elastic blocks attached by zero-thickness cohesive elements, in which the inelastic behavior of the building is concentrated, and the contact surface after detaching is defined. We used the LS-Dyna50 software due to its capacity to model explicit structural collapse and quantification of volume loss, which is a key demand parameter in this study. Illustrative representations of the numerical models developed for the three façades previously described are presented in

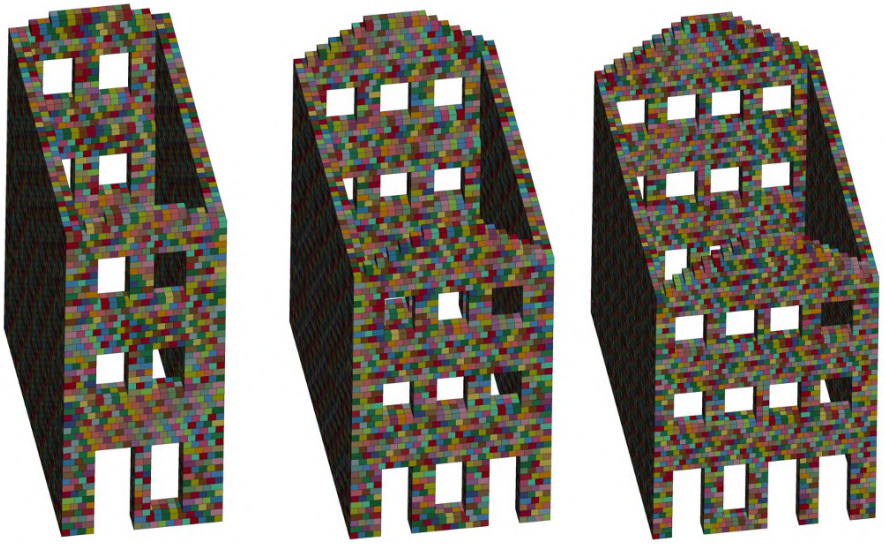

Figure 5. Sampled buildings exhibiting two, three, and four axes of openings

These numerical models allowed the simulation of several common collapse mechanisms, including the two main mechanisms previously described (i.e. "zero" and out-of-plane collapse mechanisms), as depicted in Figure 6.

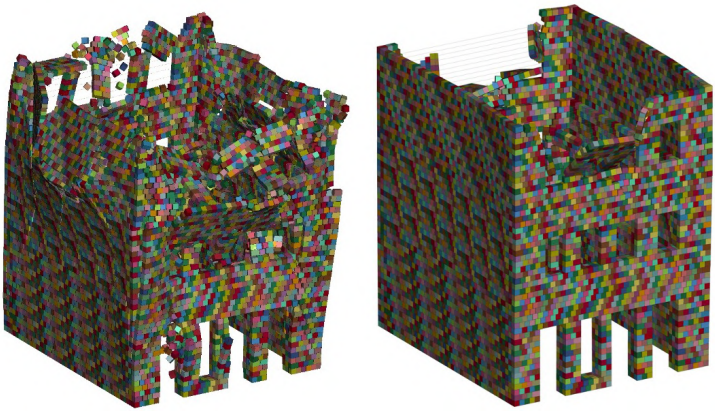

Figure 6. Examples of failure mechanisms obtained numerically for: a) "zero" collapse mechanism and b) out-of-plane collapse mechanisms in the upper storey of the front façade

Selection of Ground Motion Records

A set of 48 bi-directional ground motion records were selected from the European Engineering Strong Motion Database (ESD), considering records from stable continental and active shallow crust regions. Since the intended use of the fragility and vulnerability functions are for regional and national analysis, we avoided site-specific selection methods. Considering the tectonic environment in Portugal (e.g. Silva et al. 2014), we selected ground motion records with a moment magnitude between 5.0 and 7.5 at distances between 10 and 200 kms. The records cover intensities between 0.05 and 0.95 g of peak ground acceleration (PGA), and we aimed at a uniform distribution of PGA between this range to avoid a bias towards weaker motion. Some of the records were scaled due to the lack of recording with strong ground shaking in the ESD.

Fatality vulnerability assessment

As previously mentioned, most studies on fatality modeling use existing fragility functions (for complete or near-collapse damage states), which usually use engineering demand parameters (EDPs) such as maximum inter-storey or global drift. However, past studies indicate that the likelihood of mortality is strongly correlated with the level of destruction of the buildings, which relates well with the Internal Volume Reduction (IVR). This parameter is defined by Okada (1996) as the reduction of survival space inside the building, and it can be calculated as the plan area of the building in the first two meters. An IVR was computed for each storey by implementing an algorithm in LS-PrePost, the LS-Dyna post-processor. The algorithm calculates the volume inside the survival space before and after each dynamic analysis. For the cases where a particular storey collapsed (for example, the top floor), a value equal to 1 for the IVR was assumed. Moreover, collapse is assumed when the volume loss is higher than 60 %, as proposed by So (2016) for similar building classes. A routine was implemented in LS-Prepost53 in order to calculate both the IVR and the volume loss of structural elements.

In this project, two options for the IVR-FR relationship were used: the Abeling and Ingham (2020) linear correlation and an equation fitted to the IVR-FR data shown in the work of Spence and So (2021). The data presented by Spence and So55 considered damage and fatality observations from 47 seismic events that occurred in regions such as Europe, Latin America, United States and Asia. We fitted a numerical expression to this data using a simple least squares regression. These models are depicted in Figure 7, and both approaches were used for the development of earthquake scenarios for Portugal, as described in Section 5.

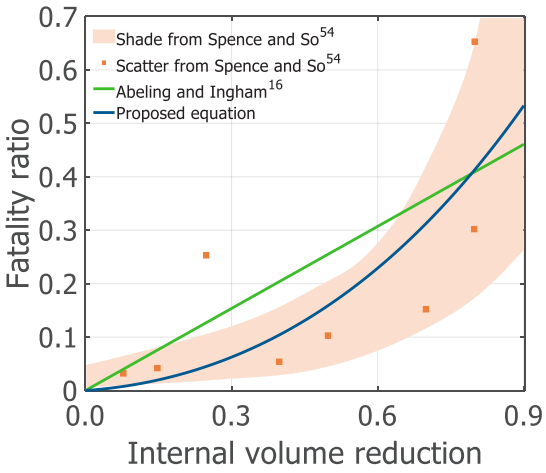

Figure 7. Fatality ratio – Internal volume loss relationships

Results

The structural response of the 8 numerical models were used to derive vulnerability functions. Approaches A and B use the relationships in terms of IM versus IVR derived in this study. However, in the first case, we used Abeling and Ingham16's model to convert IVR to FR, whereas in the second case, we used the equation fitted to the data shown by Spence and So (2021). For approaches C and D, we used the fragility functions for complete damage and collapse proposed by Lovon et al (2022) for the same building typologies, which were then converted into a probability of fatality using the ratios proposed by HAZUS. Approaches A and B aim at demonstrating the value of using an EDP (i.e. IVR) that has a strong correlation with fatalities, while methods C and D represent the conventional approach to fatality modelling, in which existing fragility functions for structural damage are adjusted. All of the fatality vulnerability functions are presented in Figure 12 and Figure 13.

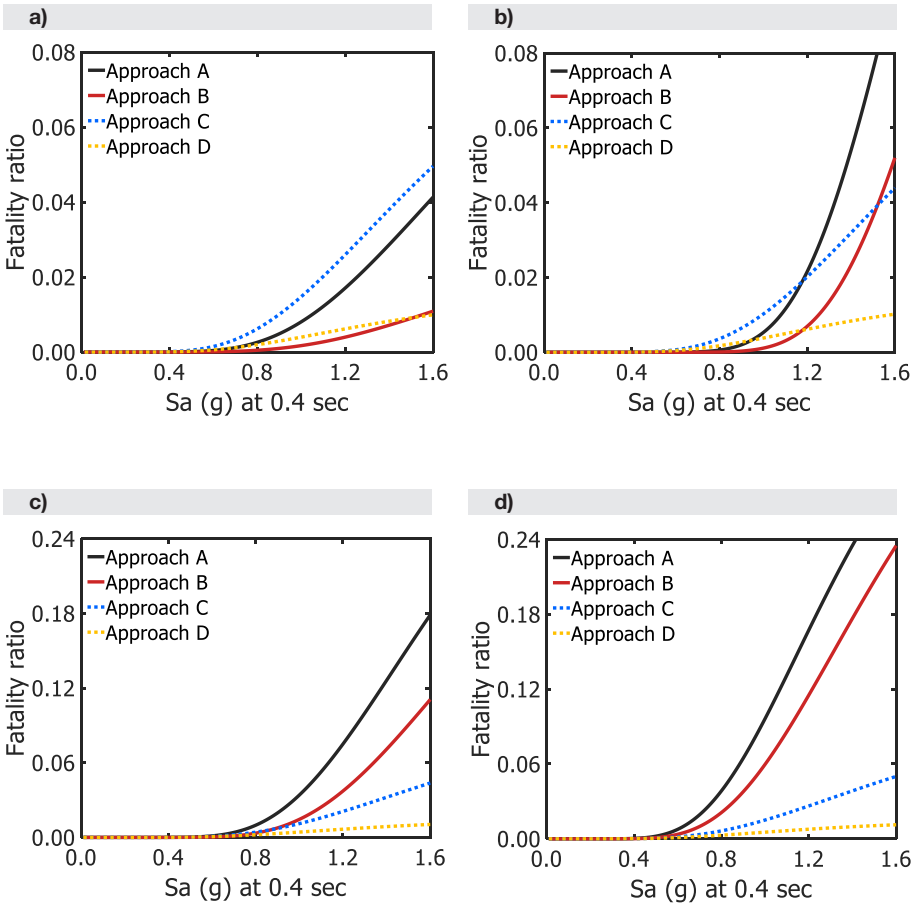

Figure 8. Fatality vulnerability functions for limestone masonry buildings of a) 1-storey b) 2-storeys c) 3-storeys d) 4-storeys

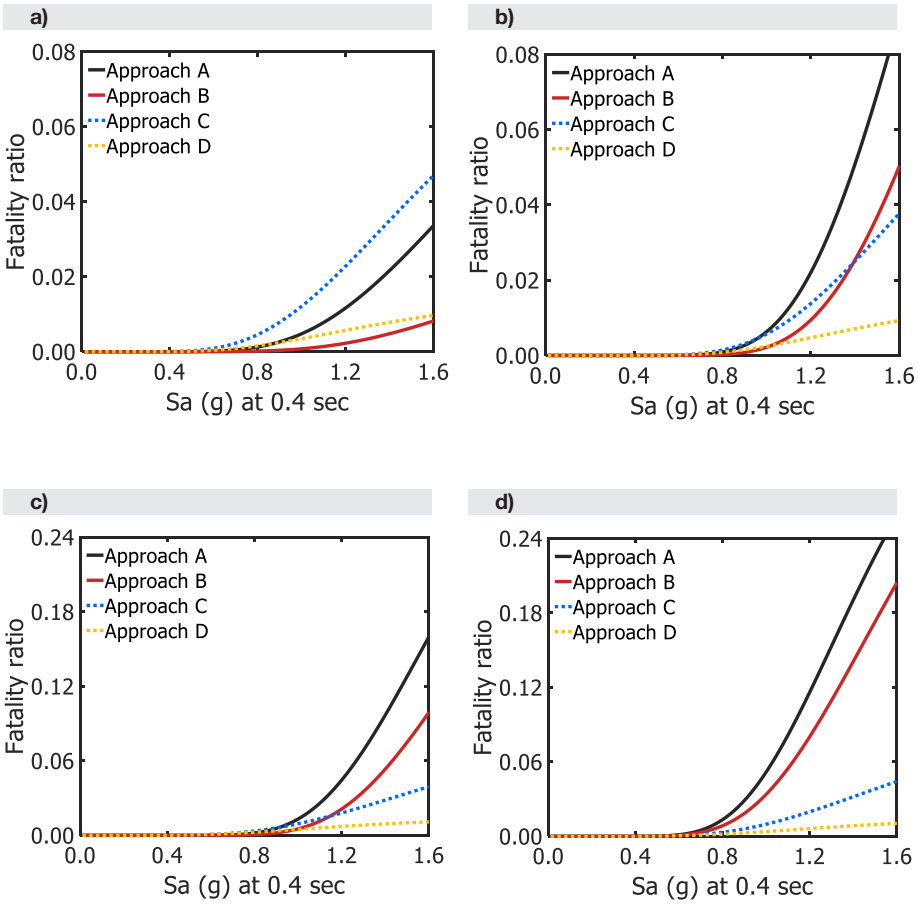

Figure 9. Fatality vulnerability functions for granite masonry buildings of a) 1-storey b) 2-storeys c) 3-storeys d) 4-storeys

In general, all methods agree on the minimum threshold level of ground shaking for which fatality rates start to increase. This is primarily due to the fact that before ground shaking values between 0.5g and 0.8g of Sa at 0.4 sec, structural damage is limited. Approach A is more conservative than approach B, which was already expected given that the linear regression proposed by Abeling and Ingham16 leads to higher fatality rates for most of the IVR values, as shown in Figure 7. The same occurs when comparing approach C with D. However, in that case, the difference can be explained by the use of the collapse rates from HAZUS in approach D (which limits the probability of collapse to a maximum value of 15%), while approach C uses directly the collapse fragility curves from Lovon et al20, which can go up to 100% probability. From these results, we argue that approach B is the most balanced and suitable method for assessing fatalities. This approach uses the IVR as the EDP, which has a stronger correlation with fatalities, and the fitted relation of IVR and FR, which despite the limited data, leads to a better fit (refer to Figure 7). These functions were used throughout this project to calculate structural damage, economic losses and human losses.

CHAPTER V

05.

A Ground Motion Model Using Machine Learning

A Ground Motion Model Using Machine Learning

A ground motion model (GMM) is fundamental for the assessment of seismic hazard and risk for a given region. These models identify the variability of earthquake intensity at different sites as a function of earthquake magnitude, source-to-site-distance, and soil conditions. For regions defined as Active Shallow Crustal (ASCR) or Subduction tectonic zones (e.g., Delavaud et al. 2012), there are dozens of empirical models due to the abundance of ground motion data (e.g., Ambraseys et al. 2005; Akkar and Bommer 2010; Zafarani et al. 2018). For regions often classified as Stable Continental Regions (SCR) such as Western Iberia, the seismicity rate is considerably lower, and the paucity of ground motion recordings hinders the development of empirical models in the same manner. To overcome the lack of empirical data in SCR, in the 1980s seismologists started developing methods to generate ground motion records compatible with these regions. The most common approaches include random vibration theory (Hanks and McGuire 1981) and stochastic simulations (Boore 1983, 2003).

The current study aims at developing a stochastic-based GMM for Western Iberia. The study area comprises mainland and offshore Portugal and Southwest of Spain. This region is located near the Azores-Gibraltar plate boundary which separates the Eurasian and the Nubian plates. Despite the relatively low seismicity, this region

has generated large magnitude events such as the 1755 M~8.5 Lisbon earthquake or the 1969 M7.8 Algarve earthquake (Vilanova et al.2012). This region has been classified as SCR in various studies, or at least GMMs for this tectonic regime tend to lead to better predictions of ground shaking (e.g., Johnston 1996; Vilanova and Fonseca 2007, Vilanova et al. 2012, Silva et al. 2015). Due to the lack of specific GMMs, models developed for other SCRs (e.g., Atkinson and Boore (2006) for East North America - ENA) have been used in seismic hazard and risk assessment studies. Vilanova et al. (2012) investigated the adequacy of GMMs developed for ASCRs and SCRs for the prediction of spectral acceleration using recorded offshore earthquakes in Portugal (e.g., 12 February 2007 M6.0 earthquake), and concluded that GMMs for ENA tend to perform relatively well.

Seismic hazard studies for this region use the same set of GMMs (mostly from ENA) for both inland and offshore Iberia. However, findings from Diaz et al. (2016) showed that the crustal thickness in inland and offshore Iberia is in the ranges of 10-15 km and 25-35 km, respectively, which are considerably lower than the 50 km crustal thickness reported in ENA. These results might explain the low attenuation of seismic waves in Iberia described in Sousa and Oliveira (1996) and Villanova et al. (2012). Furthermore, a recent study by Vales et al. (2020) computed anelastic attenuation values around Western Iberia using the Portuguese and Spanish ground motion database, and indicated attenuation values at f =1 Hz from 80 to 200, which is much lower than what has been reported for ENA. These two important studies highlight the need to explore a specific GMM for the region.

Based on the aforementioned findings, we divided the study region into two areas: inland and offshore. All ground motion records from the Portuguese and Spanish seismic network databases (Instituto Português do Mar e da Atmosfera - IPMA and Instituto Geográfico Nacional - IGN) were collected and used to calibrate the modelling parameters for the stochastic simulations. This process led to two sets of modelling parameters (i.e., inland and offshore), with the associated aleatory variability. Then, ground motion

simulations were performed to estimate the spectral acceleration values on rock (Vs30=760 m/s) for a large number of hypothetical earthquake scenarios for the region. These synthetic records were used to train, verify, and test an Artificial Neural Network (ANN), capable of predicting ground shaking in the region with a high level of accuracy. The results of the calibrated model were compared with existing GMMs developed for other SCRs, as well as with recordings from past earthquakes in the region. This model is used in Chapter 7 for the verification of the benefits of seismic monitoring in the district of Lisbon.

Seismicity and seismic hazard in Southwest Iberia

Iberia is in the southwest of the Eurasian plate, near the collision with the Nubian plate. This tectonic environment has generated some of the highest offshore magnitude events in Europe, including the 1755 M~8.5 Great Lisbon, the 1858 M~7.1 Setubal, and the 1969 M7.8 Algarve earthquakes (e.g., Vilanova and Fonseca 2007). Destructive inland events have also occurred in the past, such as the 1531 M~6.9 Lisbon, the 1909 M6.0 Benavente, the 1954 M5.0 Albolote, and the recent 2011 M5.1 Lorca earthquakes. Significant events have also occurred in the Azores archipelago due to its location at the triple junction where the North American, Eurasian, and Nubian plates meet, but this region has been excluded from the scope of this study. All these events caused significant damage in the respective regions, and in particular the 1755 Lisbon earthquake heavily damaged or destroyed more than 50% of the building stock, and approximately 10% of the population around Lisbon perished (e.g., Oliveira 1988). According to the recent unified declustered earthquake catalogue for Europe (Danciu et al. 2020), the majority of the inland events occur at relatively shallow depths (<15 km), while both shallow and deeper (>25 km) events are common in the offshore zone, along the Eurasian and Nubian boundaries. Figure 1 presents the historical and instrumental earthquake catalogue for the region covered by this study.

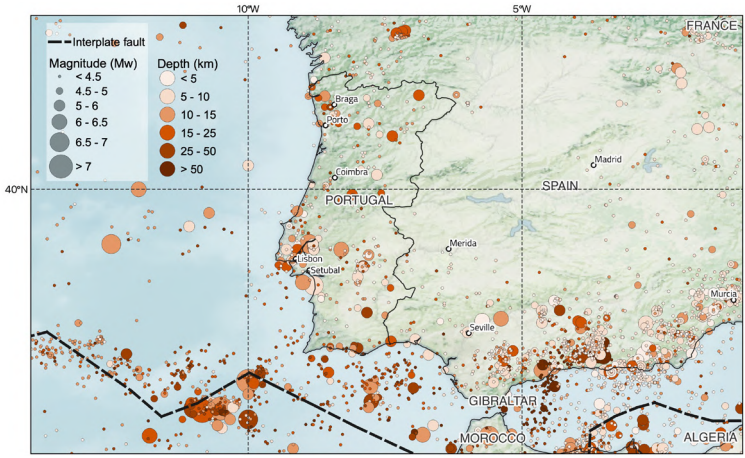

Figure 1. Instrumental and historical earthquake catalogue for Southwest Iberia (Danciu et al. 2020)

Most of the probabilistic seismic hazard models that cover this region indicate a peak ground acceleration for the 475-year return period on rock (VS30=760 m/s) between 0.15 and 0.20 g (Vilanova and Fonseca 2007, Danciu et al. 2020). However, some of these studies used ground motion models developed for ENA or active shallow regions, which could be leading to an underestimation of the seismic hazard, as later discussed in this study.

Methodology

The basis of the well-known stochastic approach for simulation of earthquake ground motion records was firstly proposed by Boore (1983). During the past decades, this method has been employed for the development of several GMMs for SCRs in different parts of the world such as ENA (Atkinson and Boore 1995, 2006), United Kingdom (Rietbrock et al. 2013), Switzerland (Edwards and Fäh 2013) and Australia (Allen 2012).

This approach follows the Brune's model for the calculation of Fourier amplitude spectra of shear waves radiated from the earthquake source, based on its seismic moment and stress (Brune 1970). Based on the predicted source spectrum, the Fourier amplitude of different frequencies can be computed at each site using an attenuation and site function. Through Equation 1, the Fourier amplitude of ground motion (A) is calculated as a function of frequency f, distance R, and seismic moment M0 of the earthquake event.

$$A(M_0, R, f) = \left(\frac{C M_0 4\pi^2 f^2}{1 + (\frac{f}{f_0})^2} \right) exp \left(\frac{exp\ exp \left[-\frac{\pi f R}{Q(f)\beta} \right]}{Z(R)} \right) exp\ (-\pi \kappa_0 f) \quad 1$$

Where f0 is the corner frequency given by, fjσ represents the stress drop (in bars) and β is the crustal shear-wave velocity (in km/s). The constantcan be computed as, where is the radiation pattern (equal to 0.55 for shear waves), F is the free-surface amplification (assumed as 2.0), V can be used to partition the groundonto two horizontal components (0.71),represents the density of the crust, and R stands for the hypocentral distance (Boore 2003). In the second term of the equation, Z(R) = is the geometrical spreading function. The coefficient n is usually assumed as 1 near the source and decreases with distance according to the Moho depth in the region. The frequency--dependent quality factor Q(f) is an inverse measure of anelastic attenuation, which depends on the region.is the diminution factor, which describes the decay of spectral amplitude at high frequencies. Since the goal of this study is to simulate large magnitude offshore earthquakes in southwest Iberia, we employed a stochastic finite--fault methodology, allowing us to take into account important finite-fault features such as the geometry of larger ruptures and its effects on the predictions. To this end, a large seismic fault is divided into a number of sub-sources and each sub-source is considered as a small point source (Hartzell 1978, Atkinson and Boore 2006). The ground motions corresponding to each sub-source are calculated

by the stochastic point-source method as explained earlier. Then, contributions from each sub-source are normalized, delayed, and summed in the time domain.

The EXSIM code (Motazedian and Atkinson 2005; Assatourians and Atkinson 2007) is used to generate synthetic ground motion records for a large suite of earthquake scenarios. EXSIM is a Fortran code which uses the stochastic finite-fault approach. To more accurately simulate the impact of finite-fault geometry on the frequency content of radiated ground motions, EXSIM employs the concept of "dynamic corner frequency," which falls over time as the rupture propagates (Motazedian and Atkinson 2005). In this section, we describe the steps that were followed to collect existing ground motion data and calibrate the modelling parameters for the simulations.

Data collection and processing

Despite the large historical events described previously, ground motion data for this region covers only events with a maximum moment magnitude of 6.0. For the case of Portugal, since the 1970s, IPMA is responsible for monitoring the seismic activity in the Portuguese territory, which covers the extensive Azores-Gibraltar plate boundary segment (Carrilho et al. 2021). Currently, 72 strong--motion stations are operated in Portugal: 4 in the Madeira Islands, 28 in the Azores, and 40 in the mainland (Carrilho et al. 2021). For the case of the Spanish territory, since 1977 the monitoring of seismic activity is managed by IGN. Using 132 stations, this seismic network collects ground motion data throughout the Iberian Peninsula, Balearics, and the Canary Islands (Amaro-Mellado et al. 2021). In this study, we used these databases to extract ground motion records for events with a minimum magnitude of 3.0 within the geographical area with longitude 16°W to 1°E and latitude 36°N to 42°N. In total, ground motion data from over 500 events were collected. Error! Reference source not found. presents the most important

earthquakes (with M > 4.5) used for the calibration of the modelling parameters.

For the processing of ground motion data, the recordings had to be corrected for the instrument response by applying appropriate filters (0.1 Hz, 30 Hz) using the open library Obspy (Beyreuther et al. 2010). The Signal to Noise Ratio (SNR) was computed for each signal by comparing the spectral amplitudes of both recorded signal (signal + noise) and pre-event signal (noise). We used a criterion of SNR greater than 3 to exclude noise from the actual recording. Figure 2 illustrates the distribution of magnitude (Mw), distance (Rjb) and depth of the resulting set of ground motion records. Despite the coverage of these national seismic networks, the recorded data from past major earthquakes is relatively scarce and only covers low-to--moderate magnitude earthquakes.

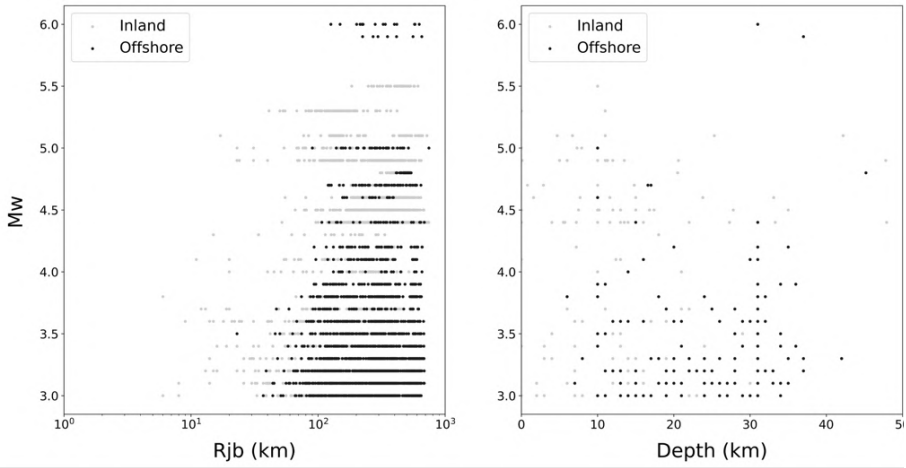

Figure 2. Distribution of magnitude (Mw) and distance (Rjb) (left) and distribution of depth (right) for the compiled earthquake catalogue

Ground motion simulations

The most relevant parameters for predicting Fourier amplitude as a function of magnitude and distance (as described in Equation 1) are the stress drop (fjσ), attenuation parameters (Z and Q), and diminution factor (κ0). By processing the ground motion records for the region, we defined statistical models for each one of these parameters. We followed closely the procedure demonstrated for regions of identical seismicity such as Switzerland (Edwards and Fah, 2013) and Australia (Allen, 2012), as described in Taherian et al. (2024). Table 1 summarizes all the parameters that were used for the stochastic ground motion simulations, along with the associated references.

Table 1. Median input parameters for ground motion simulation with EXSIM

Parameter	Median Value		Source
Crustal shear wave velocity (β)	3.5 Km/s		
Crustal density (ϱ)	2.8 g/cm^3		
Stress drop (Δσ)	50 bars (inland) 140 bars (offshore)		This study
Rupture propagation speed	0.8 β		
Pulsing percentage (%)	50%		
Kappa (κ0)	0.025		This study
Geometrical spreading function, Rn, n =	Inland -1.1 (R≤70 km) 0.2 (70 km <R≤100 km) -1.57 (R>100 km)	Offshore -1.1 (R≤115 km) -1.5 (R> 115 km)	This study
Quality factor (Q)	Q(f)=		This study
Distance-dependent duration, d R, d =	Inland 0.13 (R≤70 km) 0.09 (70 km <R≤120 km) 0.05 (R>120 km)	Offshore 0.12 (R≤115 km) 0.02 (R> 115	This study
Hypocenter location and slip duration	Random		
Pulsing percentage (%)	50		
Fault geometry	Wells and Coopersmith (1994)		
Site conditions	Rock (Vs=760 m/s)		Assumed in this study

Some of these parameters have a large aleatory variability, which must be propagated into the ground motion simulations. We calculated the variability in the geometric spreading coefficient, stress drop, and spectral decay parameters (κ0), and assumed specific probabilistic distributions as described in Table 2. For the sake of simplicity, we assumed the remaining variables as deterministic, as investigating the aleatory and epistemic uncertainty in these parameters is out of the scope of this study. To avoid unrealistic values for the spectral decay parameter (κ0) and depth of the seismic events, we adopted truncated distributions.

Table 2. Aleatory variability in key modelling parameters

Parameter	Distribution type	Mean	Standard deviation
Stress drop	Lognormal	1.70	0.30
		2.18	0.30
Kappa	Truncated normal	0.025 (0.01-0.05)	0.015
Geometrical spreading	normal	Inland	
		-1.1 (R≤70 km)	0.15
		0.2 (70 km <R≤100 km)	0.20
		-1.55 (R>100 km)	0.30
		Offshore	
		-1.1 (R≤115 km)	0.15
		-1.5 (R> 115 km)	0.30
Site conditions	Truncated normal	10 km	Inland: 13 km
		(2 km – 30 km)	
			Offshore: 20 km

Application of ANN to predict ground shaking

Different functional forms have been used in the last decades to predict ground shaking using empirical or syntethic ground motion records. In general, these expressions are comprised of 3 components (i.e., event, path and site terms) and two random variables (i.e. between and within event aleatory variability). One of the advantages of such formulations is the fact that it allows extrapolating the

preditive model to combinations of magnitude, source-to-site distance, and site conditions not necessarily well covered by the ground motion data, as each term has a physical meaning. For the study presented herein, this advantage is less relavant given that the stochastic simulation adopted herein allows generating records for all combinations of magnitude and distance. For this reason, we used the mixed-effects method (e.g., Stafford 2014) to calibrate a machine learning algorithm to predict ground shaking. In addition to the satisfacyory accuracy, uncertainty and computional performance, such models can be easily extended to the prediction of additional metrics beyond ground shaking (such as building responses).

Machine learning algorithms, and in particular Artificial Neural Networks (ANN), have been widely used in the past decade for the prediction of ground shaking (e.g., Xie et al. 2020; Derras et al. 2014). These algorithms can recognize complex nonlinear patterns in large datasets (Bishop CM 2006), and do not rely on a specific functional form. Due to the abundance of open libraries, their application to ground motion modelling is relatively straightforward, and allows the consideration of a wide range of input parameters. The neural network used in this study is a feed-forward ANN with sequential layers made up of processing units performing mathematical operations known as neurons (e.g., Haykin 2009). Each neuron is described by a collection of synaptic weights and a bias, which collectively make up the neural network's parameters. The bias is a constant that is added to the result before it is transferred to the activation function, which is shared by all neurons in a given layer, and the synaptic weights are multipliers of the outputs of the preceding layer. The objective of the ANN training is to establish the parameters of the network by minimizing a loss function, using the backpropagation algorithm.

In this chapter, the methodology described in Kalakonas and Silva (2022) was employed to train the ANN for ground motion modelling using the widely applied mixed-effects approach. This methodology follows closely the algorithm proposed by Khosravikia and Clayton (2021), with the exception of the likelihood maximiza-

tion algorithm, which is adopted from Bates et al. 2015. In particular, the ANN parameters are calculated assuming a fixed-effects regression and the random-effects, and their variances are estimated by likelihood maximization. The estimated between-event terms are substracted from the simulated ground motion data and the ANN is retrained on the updated database until the likelihood is maximized.

According to Atik et al. (2010), these random effect factors are taken to be independent random variables with standard normal distributions and standard deviations τ and φ. Regarding the determination of the ANN hyperparameters (i.e., number of hidden layers and neurons, activation functions, etc,), the methodology proposed by Kalakonas and Silva (2021) was followed. In this process, the cross-validation approach is used to split the entire database into training and testing subsets and evaluate the model's performance. In particular, a 5-fold cross validation was utilized, in which the assembled database was divided arbitrarily into 5 equal subsets (e.g., Kalakonas and Silva 2022). Five ANNs were successively trained using four folds for training and one fold for testing the model's prediction on the omitted data. The average of the five trained ANNs was used to produce the cross-validation regression metrics, providing a reliable method to identify and prevent overfittingand underfitting. Each stage and modeling decision is summarized here for the sake of clarity and reproducibility:

1. Pre-processing of input parameters and IMs: When the input and output data ranges are similar, ANN training is significantly more effective. For this reason, a one-hot encoding was used for FT while the log10 was applied to Rjb (in km), Dhyp (in km), and all IMs (in cm, cm/s, and cm/s2).
2. Optimization algorithm and loss function: The mean squared error (MSE) was selected as the loss function which was minimized by the adaptive moment estimation algorithm (ADAM).
3. Number of hidden layers and activation functions: One hidden layer was used due to its sufficiency to approximate any real function according to the universal approximation theorem (e.g., Auer et al. 2008). The hyperbolic tangent (tanh) and the

linear function were employed in the hidden and the output layer, respectively.

4. Number of neurons: The best number of neurons for the hidden layer was found by a trial-and-error process, leading to 8 neurons, while more neurons resulted in overfitting.

We trained the neural network using the open-source library TensorFlow in a Python environment (e.g., Abadi et al. 2016). Table 1 presents the average regression metrics for the 5 trained models. The evaluation of the potential over- or underfitting errors due to the choice of the hyperparameters was computed from the fixed-effect regression prior to the application of the mixed-effect algorithm. The results of the mixed-effects regression algorithm are presented in Table 2.

Table 3. Mean regression metrics of the trained ANN models using a 5-fold cross validation

T (s)	Total sigma	R^2 Training	R^2 Testing	MSE Training	MSE Testing
PGV	0.992	0.991	0.991	0.069	0.069
PGA	1.038	0.990	0.990	0.061	0.061
0.015	0.984	0.994	0.994	0.060	0.061
0.020	1.086	0.990	0.990	0.064	0.064
0.040	1.100	0.989	0.989	0.069	0.069
0.050	1.078	0.989	0.989	0.068	0.068
0.067	1.060	0.989	0.989	0.069	0.068
0.100	1.027	0.990	0.990	0.066	0.066
0.125	1.016	0.991	0.990	0.065	0.065
0.200	1.001	0.991	0.991	0.061	0.061
0.250	1.000	0.992	0.991	0.060	0.061
0.400	0.999	0.992	0.992	0.058	0.059
0.500	0.993	0.993	0.993	0.056	0.057
0.625	0.984	0.994	0.994	0.054	0.055
0.769	0.988	0.994	0.994	0.056	0.056
1.000	0.983	0.994	0.994	0.056	0.056
1.250	0.988	0.994	0.994	0.059	0.060
2.000	0.986	0.994	0.994	0.065	0.065
3.125	0.979	0.994	0.994	0.071	0.071
4.000	0.971	0.995	0.995	0.073	0.073

The R^2 coefficient is often used to measure the correlation between the recorded iMs and those predicted by the ML models. (e.g., Dhanya and Raghukanth 2018). The simulated PGA and SA(1.0s) values are displayed versus the AN"s trained values in Figure 9. The AN"s predictive power is demonstrated by the high R2 values. This strong correlation was observed across all ground shaking intensities, both during the training and testing phases. Additional analyses regarding the reliability of the resulting ground motion model are presented in the following section.

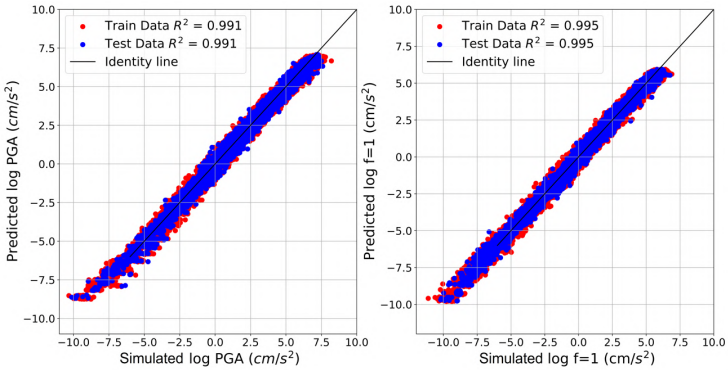

Figure 3. Stochastically simulated versus predicted correlation plot for the two selected iMs using the entire database

As previously explained, the aleatory uncertainty of the model was evaluated through the mixed-effect model. Figure 4 shows the standard deviation of the random effects versus the period of vibration (T) in sec. According to these results, the total sigma (σ) is dominated by the between-event term (τ) across all periods of vibration. This outcome contrasts with observations from empirical ground motion models in which usually the within-event term (φ) has a stronger influence in the total sigma. The reason for this discrepancy is twofold. First, in the approach presented herein, all possible combinations of magnitude and distance are considered, and for each combination different simulation parameters are sampled. This will naturally lead to a large between

even variability, as all possible outcomes will be accounted for. Cotton et al. (2013) discussed the important role of the sigma of stress drop on the between-event uncertainty (τ) suggested by different GMMs, and concluded that assuming a high uncertainty in the stress drop will lead to high between event uncertainty. Secondly, and potentially more important, all simulations in this study were performed assuming rock conditions (i.e., VS30 = 760 m/s), so the uncertainty in the site classification that is usually present in empirical models (e.g., error or bias in the estimation of VS30 values) will not exist in our analyses. We note that the same trend has been reported by various studies that also used a stochastic approach for the generation of the ground motion recordings (e.g., Edwards and Fäh 2013; Rietbrock et al. 2013).

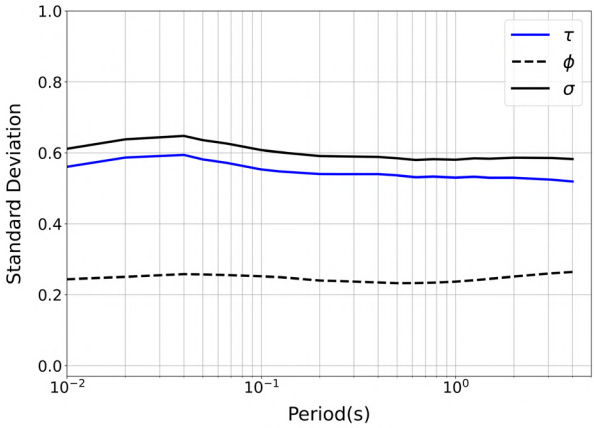

Figure 4. Standard deviation estimates of the components of aleatory uncertainty

This machine learning model to predict ground shaking in the Portuguese territory is one of the main outcomes of the ASSIMILATE project, and it was fundamental in the investigation of the identification of locations where seismic sensors should be deployed in the district of Lisbon.

CHAPTER VI

06.

The Benefits of Seismic Monitoring

The Benefits of Seismic Monitoring

In the ASSIMILATE project, we explored the benefits of installing low cost sensors to improve our knowledge and data availability about building vibrations and ground motion. We worked directly with a provider of seismic sensors that can be integrated within a seismic network. These networks are fundamental to better understand the nature and potential impact of earthquakes, as well as to plan the development of disaster risk management measures. Prior to the occurrence of destructive earthquakes, seismic monitoring can support seismologists and earthquake engineers in the development of probabilistic seismic hazard analysis (PSHA) models, calibration of ground motion models (GMMs), or the creation of earthquake scenarios. These networks can support the issuance of early warnings (e.g., Wald 2020; Cremen et al. 2022; Silva et al. 2022, 2023) or the rapid assessment of the expected economic losses, damage, and casualties (e.g., Jaiswal and Wald 2013). The former action has the potential to reduce casualties by allowing the population to pursue protective measures (e.g., McBride et al. 2022), whereas the latter can support several emergency operations. These can include the identification of regions where response teams should be deployed, advise agencies and utilities about the need to activate contingency plans, support international organizations such the World Bank, the United States Agency for International Development (USAID) or the

European Union in releasing financial support, and advise the (re) insurance industry about eventual large claims.

Numerous rapid loss assessment systems have been created in the last two decades at various scales including urban (e.g., Istanbul - Erdik et al. 2003), regional (e.g., Romanian-Bulgarian border - Erduran et al. 2012), national (e.g., Japan - Hoshiba et al. 2011; Portugal - Silva et al. 2015; United States - Wald et al. 2020), continental (Europe through the RISE project - www.rise-eu.org), and global (PAGER - Jaiswal and Wald 2010; WAPMERR - Wyss 2004). Generally, these systems rely on three primary components for estimating losses and damages: 1) an exposure model defining the spatial distribution, value, and vulnerability attributes of the assets; 2) a suite of vulnerability functions that establish the likelihood of damage or loss based on an intensity measure (IM); and 3) sets of ground motion fields or hazard footprints. The generation of the ground shaking component can be performed through various strategies, ranging from the simple application of a GMM using an epicenter estimated shortly after a seismic event (e.g., Silva et al. 2015) to more intricate processes that integrate data from seismic stations to reduce bias and uncertainty in resulting losses (e.g., Engler et al. 2022).

The estimation of the ground shaking is undeniably the most influential and constrainable factor (Crowley et al. 2008; Kalakonas et al. 2020). Several studies have evaluated the influence of the epistemic and aleatory uncertainty from the GMMs in earthquake scenarios (e.g., Fiorini et al. 2012, Silva 2016), and concluded that the former can lead to differences in the loss results by a factor of 2 to 4, while the latter (i.e., sigma from the GMMs) can cause a variability in the losses of 1 order of magnitude. Fiorini et al. (2012) calculated the number of unusable buildings (on soil) and indicated values ranging from 1,000 to nearly 45,000 buildings. This large variability in impact estimates renders the results less useful for most purposes. A localized impact might be dealt by local authorities, while a more widespread impact might require assistance from the central government or even the international community. Using the example for Italy, 1,000 unusable buildings could translate into 3,000 people left

homeless, while 45,000 could represent more than 100,000 people displaced.

It is thus important to explore methods to reduce the uncertainty and bias in the estimation of the ground shaking. Worden et al. (2018), Silva and Horspool (2019), and Engler et al. (2022) discuss how data from seismic stations can be combined with spatial and inter-period correlation models to improve the reliability of ground shaking fields. However, the performance of these methods depends heavily on the density and reliability of the seismic network in the affected area. Dense seismic networks are rare and only exist in specific parts of the world (e.g., China, Italy, Japan, Taiwan, New Zealand, the west coast of the United States). Typically, less than ten stations exist in any given region, or even none in less-developed nations. The lack of seismic stations is partially due to the costs of installing and maintaining a large network, but the rise in low-cost sensors might change how rapid loss assessment systems can be designed. Notwithstanding the significant costs in maintaining real-time operations and data archiving and distribution, this new technology might allow the installment of dense networks in regions that are currently poorly monitored.

We demonstrate the impact of integrating data from increasingly dense networks in the assessment of ground shaking, damage, and losses. Due to the lack of ground shaking data for Portugal, to demonstrate these benefits within ASSIMILATE, we used ground motion recordings from the 1999 M7.7 Chi-Chi and ground motion fields generated using stochastic simulations (e.g., Boore 2003; Motazedian and Atkinson 2005; D'Amico et al. 2012) for Taiwan. We evaluated the reduction in the estimation error of the event bias and ground shaking, considering seismic networks with different densities. In the following chapter, we demonstrate this technology considering economic losses and damages for the district of Lisbon (Portugal).

Integrating seismic stations data in ground motion fields

As previously discussed, the main source of uncertainty in the evaluation of earthquake impact scenarios is definitely in the ground shaking component (e.g., Crowley et al. 2008; Silva 2016). Two sources of uncertainty characterize this process: epistemic and aleatory. The former is related to our lack of knowledge or data regarding the expected ground shaking in the region, and it is usually incorporated in earthquake scenarios by considering multiple GMMs. Alternatively, a GMM (backbone model) that depends on different parameters (that are region-dependent) can be used, as recently proposed for the European territory (Kotha et al. 2020). In theory, with additional information, this source of uncertainty could be reduced. The second type of uncertainty is related to the randomness of the ground shaking process, and it cannot be completely reduced. A ground shaking intensity measure (IM) at a given site is usually calculated through the following expression:

$$\mathrm{Log}(IM)=\mu(M,R,\theta)+\zeta \qquad (1)$$

Where IM represents an intensity measure such as peak ground acceleration (PGA), peak ground velocity (PGV), spectral acceleration (SA), amongst others. $\mu(M,R,\theta)$ stands for the mean logarithm of the IM, as a function of the magnitude (M), a measure of distance (R) and other parameters (θ) like site conditions or faulting mechanism. ζ represents the total residual of Log(IM). By treating the the total residual as a linear mixed-effects model (Abrahanson and Youngs 1992; Engler et al. 2022), equation (1) can be adjusted as follows:

$$\mathrm{Log}(IM)=\mu(M,R,\theta)+B+W \qquad (2)$$

Where B represents the between-event residual (i.e., representing the variability in the ground shaking amongst events with the same

magnitude) and W stands for the within-event residual (i.e., representing the variability within the same event, for sites at the same distance and soil conditions). These residuals usually follow a normal distribution, and for the assessment of earthquake damage or losses, they can be randomly sampled using Monte Carlos simulations or numerically integrated using the respective standard deviations associated with each GMM.

Preferably, a dense network of recording stations would exist in the areas heavily affected by damaging earthquakes that would enable loss modelers to estimate the expected impact with limited uncertainty in the ground shaking. In such idealized situations, GMMs or a rupture model would not be necessary. In reality, the density of seismic networks is frequently insufficient, even in countries with well-developed networks (assuming the station data are all immediately available, which has not always been the case). In these cases, it is necessary to use GMMs to calculate ground shaking in locations far from seismic stations. However, as discussed in the literature on this topic (Worden et al. 2018; Silva and Horspool 2019; Engler et al. 2022), cross-spatial correlation models can be employed to infer the ground shaking at sites without a station nearby.

In ASSIMILATE, we evaluated the benefits of integrating data from seismic stations in the calculations of ground shaking, building damages and economic losses considering different seismic events and seismic network densities. In our evaluation, we considered several seismic events and calculated the mean between-event (μB) term (also known as the event bias) for each event and each IM based on data from seismic stations (real or hypothetical),

For the evaluation of the benefits of incorporation data from dense seismic networks, ground motion recordings caused by strong earthquakes in regions with hundreds of seismic stations should be used. However, except for a few examples, such cases are rare. In this section, we demonstrate how the error in the estimation of the ground shaking and the between-event term (μBk)) can be significantly reduced with a sufficient number of seismic stations for two examples: 1) considering the ground motion data recorded in

the 1999 M7.7 Chi-Chi (Taiwan) earthquake, and 2) by generating thousands of ground motion fields for Taiwan using a seismic hazard model (Chan et al. 2020) and stochastic simulations (e.g., D'Amico et al. 2012).

Application to the 1999 M7.7 Chi-Chi (Taiwan) earthquake

The 1999 M7.7 Chi-Chi earthquake was a shallow event produced by the Chelungpu thrust fault, whose ground shaking was recorded by more than 400 seismic stations distributed throughout the island (Ji et al. 2003; Zhang et al. 2010). This event has been the subject of dozens of ground motion modeling and loss assessment studies due to the availability of information regarding the seismic stations, the associated ground motion recordings, and the loss and damage impact. In this chapter, we used the seismic station data available in the USGS ShakeMap Atlas (Marano et al. 2023), which covers 421 stations for this event (see Figure 1a). We used the global GMM of Cauzzi et al. (2015), the spatial correlation model from Jayaram and Baker (2009), and the inter-period correlation model from Goda and Atkinson (2009) to estimate the mean between-event (μB) term for this event. We used the earthquake rupture geometry proposed by Ji et al. (2010), which is comprised of three fault segments, as illustrated in Figure 1. The accurate estimation of this bias requires a large number of records with a particular spatial distribution (Crowley et al., 2008; Stafford 2014). In other words, a reduced number of records might lead to an under or over-estimation of this bias, and consequently to a miscalculation of the associated impact. Given the large number of observations for the Chi-Chi earthquake, we assumed that the μB calculated using the recordings from the entire seismic network is the "true" bias for each IM for this event. To test how the incorporation of an increasing amount of data from seismic stations can improve the estimation of the bias and ground shaking

in the region, we consistently separated the data from the 421 stations into two groups: 1) observations – comprised of up to 50 stations, and 2) target sites – comprised of 371 locations. This split was randomly performed hundreds of times to consider different spatial distributions of the two groups (see Figure 1b) for an illustration of a random generation of the two groups).

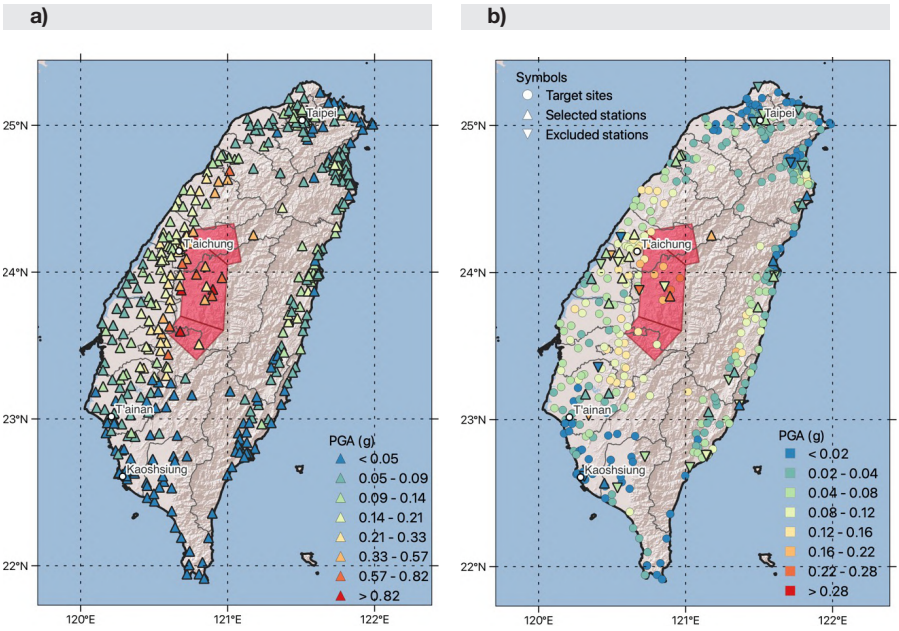

Figure 1. a) PGA recorded at 421 stations during the 1999 M7.7 Chi-Chi (Taiwan) earthquake. The vertical projection of the seismic rupture is represented by the red rectangle, following the geometry proposed by Ji et al. (2003). b) estimated ground shaking (PGA) at the target sites (represented by circles), conditioned on 25 seismic stations (upwards triangles). The 25 stations that also belonged to the pool of 50 observations but were not considered in the estimation of the ground shaking are represented by downwards triangles

We estimated the error in the calculation of the mean bias (εμB) and ground shaking (εIM) with an increasing number of seismic stations. The error in the mean bias was computed by comparing the estimated bias with the "true" bias (i.e., considering all seismic stations in the region). The error in the ground shaking was computed by comparing the estimated ground shaking with the recorded shaking at the target sites. As previously mentioned, to test different spatial distributions of observations, we randomly generated 100 realizations of the two groups (observations and target sites). For the case of the ground shaking error, we also considered a case where no stations are considered (i.e., unconditioned ground shaking). This case allows investigating the potential error when estimating ground shaking with no data from recording stations. This is typically the case in regions with no seismic networks, or when estimating ground shaking shortly after the occurrence of earthquakes, when the data might still be inaccessible. The distribution of εμB and εIM are presented in Figure 2 for PGA using whisker plots to properly illustrate the entire distribution of the absolute errors.

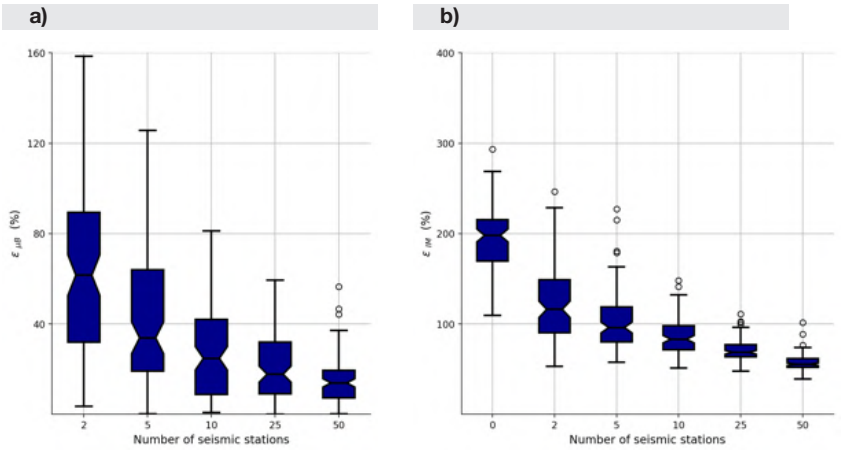

Figure 2. Whisker plots illustrating the statistical distribution of: a) error in the estimation of the mean event bias (εμB) and b) error in the estimation of the PGA at the target sites (εIM)

The statistical distribution of the error in the bias and ground shaking estimation indicates a significant decrease with at least 10 stations in the region, and only minor benefits with a number of seismic stations above 25. For the specific case of μB, there are currently no recommendations in the literature regarding the minimum number of recordings that should be used to define this fundamental parameter (e.g., Crowley et al. 2008), but in our analyses, 25 stations were sufficient to obtain an estimate with a median error below 15%. In terms of ground shaking, we note that not conditioning the ground shaking leads, on average, to errors above 150%, while including at least 2 stations reduces this error by almost half. More importantly, we noted that increasing the number of stations does not cause a significant reduction in the ground shaking error. In fact, for the case of 50 seismic stations, the average error is still in the order of 60% for PGA. Such large differences between the estimated and observed ground shaking can cause a severe under- or over--estimation of the associated impact, as later demonstrated in this study. We investigated the potential causes for the large εIM, even when incorporating data from many seismic stations. We observed that target sites without a seismic station within a 10 km radius tend to have a median εIM above 60%. This trend is illustrated in Figure 3, where the results considering 50 (random) seismic stations are presented. The left panel shows the distance between each target site and the closest seismic station, while the right panel shows the median εIM for each target site.

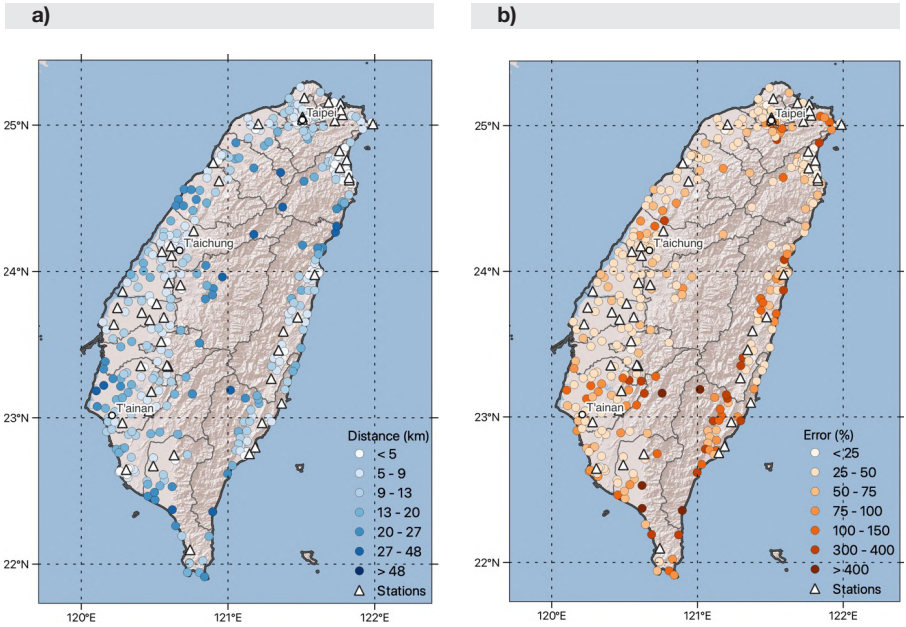

Figure 3. a) Distance between the target sites and the closest seismic station, and b) median error in the estimation of the ground shaking at the target sites, conditioned on the 50 seismic stations

The evaluation of the error with the distance to the closest seismic station indicates that dense networks might be necessary to accurately assess the ground shaking in the affected region, in particular for the rapid assessment of damages and losses, as further discussed in Section 3. Whilst the findings presented in this section are useful, they obviously represent a single seismic event, and are conditional on the previously described modelling assumptions (e.g., ground motion models, seismic rupture geometry, correlation models). In the following section, we performed the same tests, but considering hundreds of seismic events randomly generated using a probabilistic seismic hazard model for Taiwan and stochastic simulations to compute the hypothetical ground shaking.

Application considering probabilistic seismic hazard for Taiwan

In this section we aim at evaluating the benefits of seismic monitoring in the estimation of ground shaking, considering hundreds of events with different characteristics, as well as a number of stations spanning from zero (i.e., no stations - unconditioned ground shaking) to 421 (i.e. the entire seismic network of Taiwan, according to the network configuration at the time of the 1999 M7.7 Chi-Chi earthquake). We used the probabilistic seismic hazard model from Chan et al. (2020) for Taiwan and the OpenQuake-engine (Pagani et al. 2014) to generate 1,000 years of seismic events with a minimum moment magnitude of 5.25, as depicted in Figure 4. Since ground motion recordings for all the generated events do not obviously exist, we used the EXSIM code (Motazedian and Atkinson 2005) to perform stochastic simulations and compute the spatial distribution of ground shaking in the entire country, as summarized in this section.

EXSIM is a stochastic finite-source simulation algorithm available as open-source code, which generates synthetic ground motion records for specific earthquake scenarios (e.g., Motazedian and Atkinson 2005; Assatourians and Atkinson 2007). The methodology involves dividing a fault plane, sized according to its seismic moment, into an array of subsources. Each subsource is treated as a point source, and time series from these subsources are simulated using the point-source stochastic model developed by Boore (1983, 2003). The model simulates ground motion using random Gaussian noise with a specified duration and an underlying spectrum derived from the Brune (1970) point-source model. The resulting time series from all subsources are combined in the time domain, considering appropriate time delays for rupture front propagation (Atkinson and Assatourians, 2015). Brune's model defines the Fourier spectrum based on seismic moment (M0) and stress drop (fjσ), with attenuation in the frequency domain according to an empirical model. This empirical attenuation model characterizes the path effects, and it is composed of two components: geometrical spreading (G) and ane-

lastic attenuation (Q). The first term describes the ground motion attenuation as a function of distance, while the latter is a frequency--dependent attenuation parameter. The spectra are additionally attenuated using a spectral decay parameter (κ).

There have been several studies to calibrate the modelling parameters for stochastic simulation for earthquakes in Taiwan. Some of these studies used stochastic simulations to find the best estimate of key modelling parameters to simulate specific events, such as the 1999 M7.1 Chi-Chi earthquake (Roumelioti and Beresnev 2003), the 2013 Nantou earthquake (Joshi et al. 2015), and the 2016 Meinong earthquake (Chen et al. 2017). We adopted the modelling parameters proposed by D'Amico et al. (2012), whose results were calibrated considering data from 170 aftershocks from the Chi–Chi earthquake. The simulated spectra were amplified using the site amplification model developed by Chao et al. (2019) for Taiwan. Table 1 summarizes the input parameters for the stochastic simulations.

Table 1. EXSIM input parameters for ground motion simulation for Taiwan (D'Amico *et al.* 2012)

Damage State	Loss Ratio (LR) (%)
Crustal shear wave velocity (β)	3.2 Km/s
Crustal density (ϱ)	2.8 g/cm3
Stress drop (Δσ)	60 bars (Mw <= 5.5) 80 bars (5.5 < Mw < 7.0) 90 bars (Mw >= 7.0)
Rupture propagation speed	0.8 β
Pulsing percentage (%)	50%
Kappa (κ0)	0.05 s
Geometrical spreading function, Rn, n =	60 bars (Mw <= 5.5) 80 bars (5.5 < Mw < 7.0) 90 bars (Mw >= 7.0)
Quality factor (Q)	Q (f) = 350.0 $f^{0.32}$
Distance-dependent duration, d R, d =	0.05
Hypocenter location and slip duration	Random
Pulsing percentage (%)	50

We estimated ground shaking at the location of every seismic station, as well as on an evenly spaced grid with a 4x4 km2 spatial resolution covering all districts of Taiwan. To improve the computational performance, locations with fewer than 100 people (according to the population dataset WorldPop) were excluded. This led to a total of 1232 sites where ground shaking was calculated. Moreover, we also excluded events that did not generate significant ground shaking or that were located too far from Taiwan. As an example, Figure 4 illustrates the ground shaking (in terms of PGA) for a seismic event with a moment magnitude of 7.1 in the Longitudinal Valley fault.

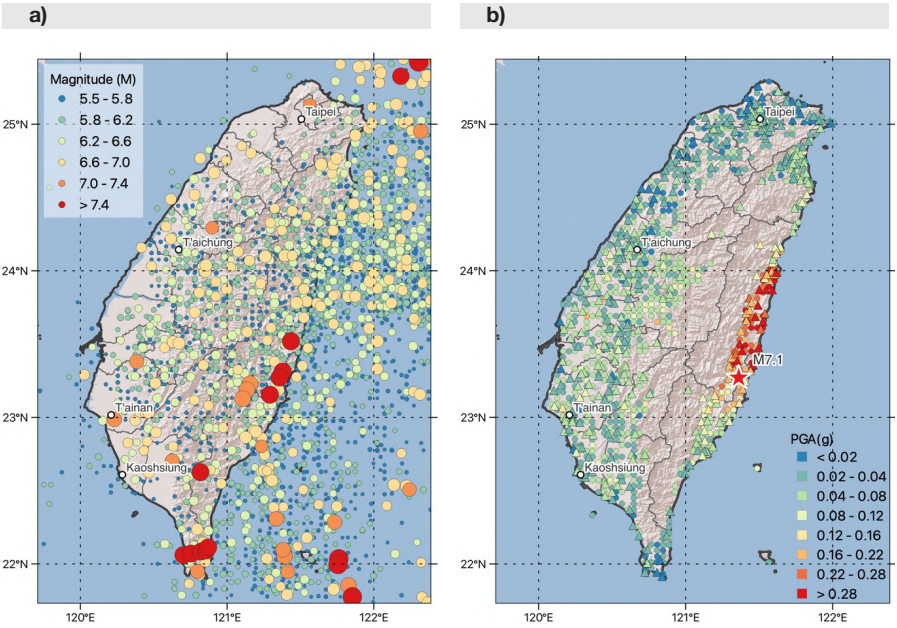

Figure 4. a) Stochastic event set for Taiwan using the seismic hazard model proposed by Chan et al. (2020) and b) ground shaking (in terms of PGA in g) at the target sites (represented by circles) and seismic stations (represented by the triangles) for a M7.1 event located in the Longitudinal Valley fault

Each ground motion field generated using the stochastic simulation was assumed as the "true" ground shaking caused by the associated event. Likewise, the event bias was calculated considering the shaking at the 1232 sites and assumed to be the "true" bias. Then, a different number of seismic stations was considered to condition the shaking in the region, using the same ground motion and correlation models described in the previous section. We compared the event bias μB (estimated using a given number of seismic stations) with the "true" bias, and the estimated ground shaking (conditioned on a given number of seismic stations) with the "true" ground shaking at each site. The resulting the errors ($\varepsilon_{\mu B}$ and ε_{IM}) are presented in Figure 5.

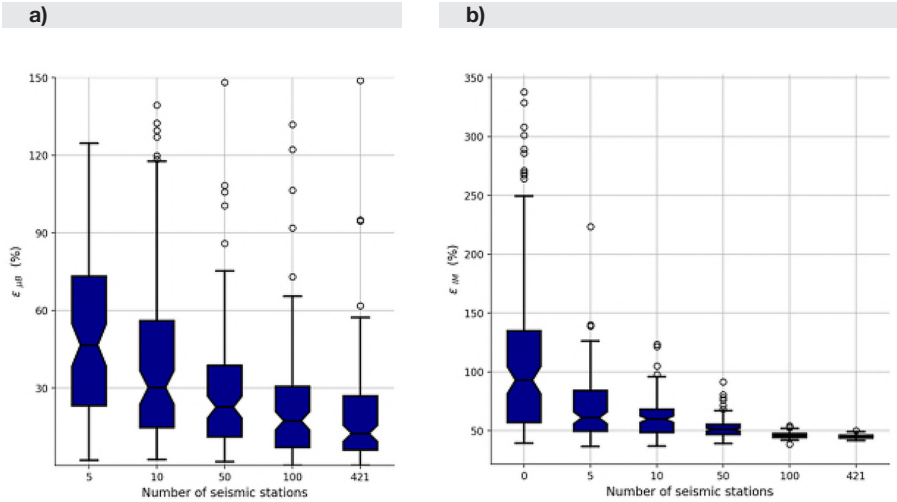

Figure 5. Whisker plots illustrating the statistical distribution of: a) error in the estimation of the mean bias (εμB) and b) error in the estimation of the ground shaking at the target sites (εIM)

The results using the stochastic event set for Taiwan indicate a clear reduction in both errors, in particular in the estimation of the event bias μB. The error in the estimation of the ground shaking εIM, indicates practically no benefit with an increase from 100 to 421 stations. To properly understand this rather surprising finding, it is important to recognize that the error in the estimation of ground shaking at each site depends on the adjustment of both the between (B) and within-event (W) terms of the ground motion model, as described by Equation (2). For the former term, it is clear from Figure 5a that 100 stations are already sufficient to estimate the event bias, so adding more stations barely improves the adjustment of B. The within-event term, as previously explained, can only be reduced if a nearby station exists. In Taiwan, seismic stations are naturally concentrated in populated places, with some stations less than two kilometers apart in cities such as Taipei, Kaohsiung, Hualien, or Taitung. This spatial configuration means that when the number of stations is increased beyond 100, it is often the case that identical ground motion data is being added to the estimation process, which does not necessarily improve the adjustment of W for sites with no seismic stations nearby. In fact, 32 % of the target sites do not have a seismic station within a radius of 5 km, which is a distance beyond which the spatial correlation in the ground motion residuals decreases significantly for PGA and Spectra Acceleration at short periods (e.g., Goda and Hong 2008; Jayaram and Baker 2009). This finding does not mean that the seismic stations in Taiwan are somehow redundant or that their distribution is illogical. In this exercise all sites are assumed as equally important in the estimation of εIM, while obviously some areas have greater population and more building and infrastructure, and thus should be better monitored. The appraisal of the benefits of seismic monitoring should also consider what exists at each site if loss estimation is a priority, as explored in the following section.

CHAPTER VII

07.

Designing a Rapid Loss Assessment System in Portugal

Designing a Rapid Loss Assessment System in Portugal

The previous chapter demonstrated the benefits of seismic monitoring in the reduction of the error in the ground shaking estimation. In this chapter, we extend that study to the evaluation of the potential benefits in reducing the error in the impact assessment. One of the reasons for conditioning ground shaking (as performed by the USGS ShakeMap system – Worden et al. 2018) is the potential to improve the assessment of economic losses, damages, and fatalities (e.g., Silva and Horspool 2019), particularly in the hours or days after the occurrence of destructive events. These potential benefits are visible in the evolution of the economic and loss estimates issued by the USGS PAGER system (Wald et al. 2008), which get closer to the reported impact once data from seismic networks is incorporated in the impact assessment (Wald et al. 2022).

In this part of the ASSIMILATE project, we quantified the potential error in the estimation of economic losses, damages, and fatalities considering the district of Lisbon, Portugal, with the aim to explore the benefits of dense networks in large urban centers, whose seismic stations can be strategically allocated to maximize resources. The following sections describe the various components of the impact analysis and the methodology to test this hypothesis. Then, we explore different strategies to distribute sensors in the region of interest, and discuss the proposed design for the system for Lisbon.

Exposure and vulnerability models

Damage and loss assessments require an exposure model of the region of interest, a set of vulnerability or fragility functions, and one or multiple ground shaking fields. We used the exposure model originally described in Chapter 2. This model was developed using housing and socio-economic data from the 2011 and 2021 housing census, and it characterized the building stock at the smallest available administrative division ("freguesia"). This model was then further disaggregated on an evenly spaced grid following a 0.02x0.02 decimal degrees spatial resolution. For the vulnerability component, we employed the vulnerability functions from the global vulnerability database of the Global Earthquake Model (GEM - Martins and Silva 2020) for the reinforced concrete building stock and the unreinforced masonry vulnerability functions described in Chapter 4. All models are publicly available through repositories as described in the associated publications. The economic value and number of buildings at the third administrative level for the Lisbon district are presented in Figure 1. These maps indicate an accumulation of the economic value of the building stock in the south of the district, where taller and more modern buildings are frequent in the municipalities of Lisbon, Cascais, Sintra, and Oeiras. In contrast, the distribution of the number of buildings, regardless of their cost, is more uniformly distributed, with significant concentrations in the western part of the district, in the municipalities of Cascais, Sintra, Mafra, and Torres Vedras. The spatial distribution of the building stock and population is critical when considering a strategic distribution of seismic stations, as demonstrated in this section.

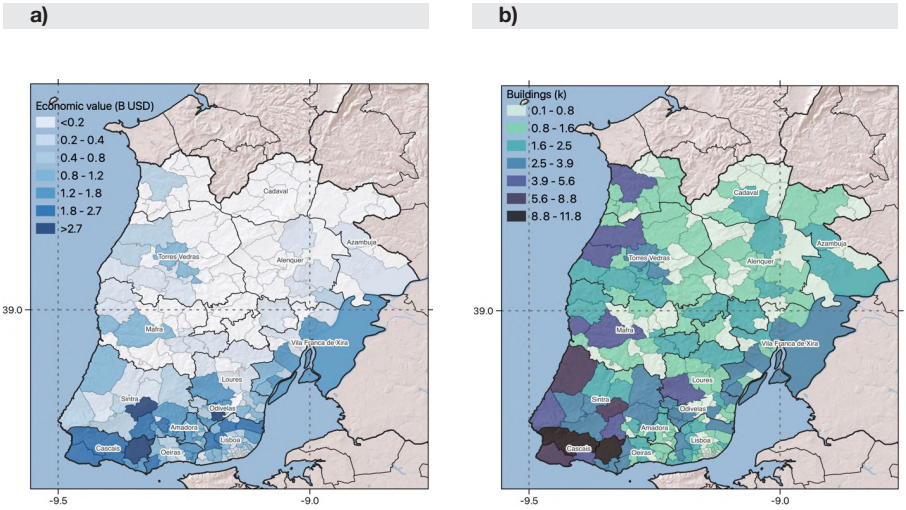

Figure 1. Spatial distribution of: a) economic value (in billion USD), and a) number of buildings (in thousands) at the third administrative level (i.e., freguesia)

Ground shaking estimation and conditioning

We randomly sampled 10,000 years of earthquake ruptures with a minimum moment magnitude of 5.25 around the Lisbon district using the European Seismic Hazard Model (ESHM20 – Danciu et al. 2021) and the OpenQuake-engine (Pagani et al. 2014). Given the lack of ground motion recordings for Portugal, we followed the same stochastic simulation approach described in Chapter 5 for the generation of the ground motion fields. We computed ground shaking on an evenly spaced grid with a 2x2 km2 spatial resolution. To improve computational performance, locations with fewer than 100 people (according to the population dataset WorldPop) were excluded, leading a total of 1,114 sites. Ground shaking was also calculated at the locations of the 7 seismic stations currently installed in the district of Lisbon (see Figure 7), as part of the national seismic network

(Carrilho et al. 2021). Again, we excluded events that did not generate significant ground shaking. The modelling parameters were specifically derived for Western Iberia, as described in Taherian et al. (2024), and summarized in Table 2.

Table 2. Modelling parameters assumed for the ground shaking stochastic simulations for the Lisbon District

Parameter	Median Value
Crustal shear wave velocity (β)	3.5 Km/s
Crustal density (ϱ)	2.8 g/cm^3
Stress drop (Δσ)	50 bars (inland) / 140 bars (offshore)
Rupture propagation speed	0.8 β
Pulsing percentage (%)	50%
Kappa (κ0)	0.025
Geometrical spreading function, Rn, n =	Inland -1.1 (R≤70 km) 0.2 (70 km <R≤100 km) -1.57 (R>100 km) Offshore -1.1 (R≤115 km) -1.5 (R> 115 km)
Quality factor (Q)	Q (f)
Distance-dependent duration, d R, d =	Inland 0.13 (R≤70 km) 0.09 (70 km <R≤120 km) 0.05 (R>120 km) Offshore 0.12 (R≤115 km) 0.02 (R> 115 km)
Hypocenter location and slip duration	0.13 (R≤70 km)
Pulsing percentage (%)	0.09 (70 km <R≤120 km)
	0.05 (R>120 km)

Figure 2. a illustrates the generated stochastic event set around the district of Lisbon, while Figure 2b presents one realization of the distribution of PGA for a random event, with an epicenter and magnitude identical to the historical 1909 M6.0 Benavente earthquake. For each sampled event, we assumed that the ground shaking generated using the stochastic simulation is the "true" ground shaking for that event.

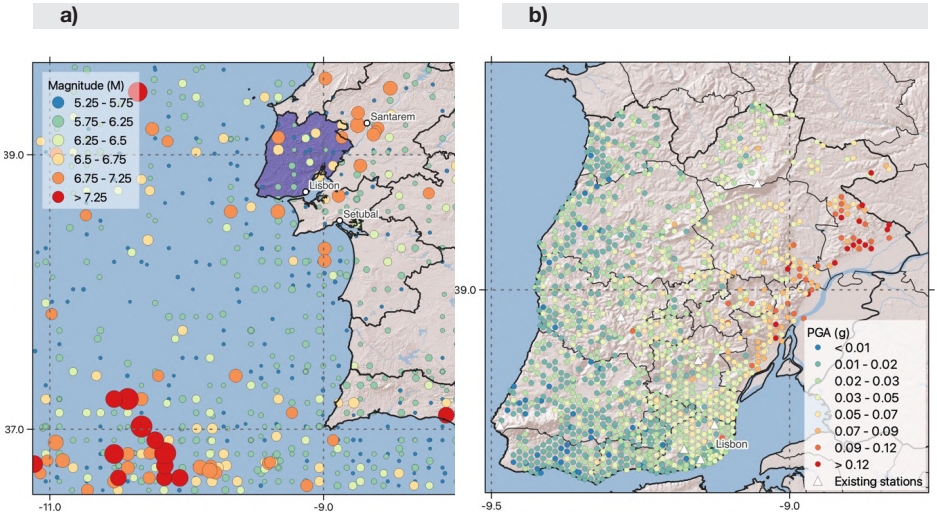

Figure 2. Stochastic event set for a region around the district of Lisbon using the seismic hazard model proposed by Danciu et al. (2021) and b) ground shaking (in terms of PGA in g) at the target sites (represented by circles) for an hypothetical earthquake with a location and magnitude identical to the historical 1909 M6.0 Benavente earthquake. The existing seismic network in the district of Lisbon is represented by the white triangles

Evaluation of the benefits of seismic monitoring in impact assessment

For each sampled event, we calculated the economic losses, number of collapsed buildings, and fatalities using the "true" ground shaking. Then, for the evaluation of how the incorporation of data from seismic stations could improve the accuracy of the impact assessment for the region, we followed the steps below:

1. The "true" ground shaking at the location of the seismic stations was collected and assumed to be the only ground motion data available shortly after the occurrence of an

earthquake (along with the epicenter, magnitude, and moment tensor).

2. Using the estimated seismic rupture (i.e., epicenter, magnitude, and geometry based on the dip, rake and strike angles), the data from the seismic stations, one ground motion model, and a spatial and inter-period correlation model, we generated 100 realizations of conditioned ground shaking in the district. We used the Akkar et al. (2014) GMM and the same correlation models previously described. We generated conditioned cross-correlated ground motion fields for PGA and spectral acceleration (SA) at 0.3, 0.6 and 1.0 seconds (i.e., the intensity measures used by the vulnerability models).
3. Using the ground shaking conditioned on the data from the seismic stations, we calculated the same loss metrics (i.e., economic losses, number of collapsed buildings, and fatalities).
4. We compared these loss metrics with the ones calculated using the "true" ground shaking to evaluate the reduction in the error due to the incorporation of seismic station data.

As presented in the previous chapter, we considered an increasing number of seismic stations in the region to evaluate how the error decreases with the additional ground motion data. However, for the assessment of losses, it is illogical to distribute (hypothetical) seismic stations randomly. It is expected that a seismic network will have a greater number of stations in populated places, or where important infrastructure exists. In this study, we spatially distributed the seismic stations proportional to five exposure or risk metrics as listed below:

1. Economic value of the building stock.
2. Number of buildings.
3. Population.
4. Number of vulnerable buildings.
5. Earthquake risk.

For the fourth criterion, we considered unreinforced masonry buildings and reinforced concrete structures without seismic provisions as the vulnerable buildings. For the last criterion, we used the average annualized economic losses (AAL) for Portugal, calculated within the

scope of the Global Seismic Risk Model of GEM (Silva et al. 2020 – see country profile at https://github.com/gem/risk-profiles/tree/master/Europe/Portugal). In this process, n number of (hypothetical) seismic stations are assigned to the n grid cells with the highest value of the associated metric, while maintaining a minimum distance of 5 km between stations. The resulting seismic networks considering 2, 5, 10 and 20 stations distributed according to the 5 criteria are illustrated in Figure 3.

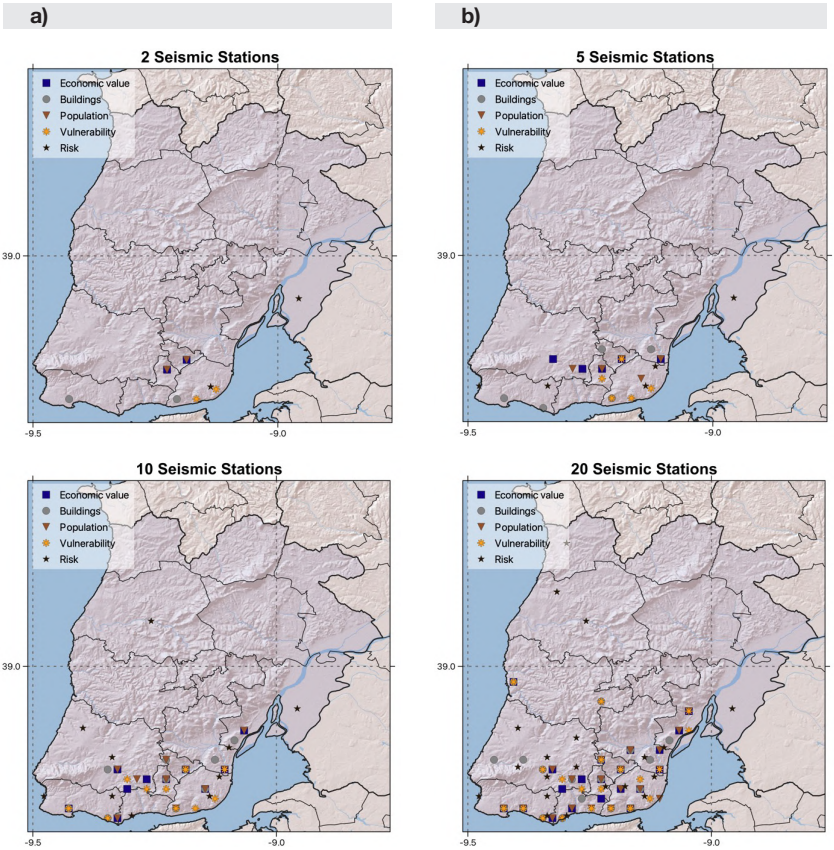

Figure 3. Distribution of hypothetical seismic stations considering five criteria (economic value, buildings, population, vulnerability, and risk) and an increasing number of stations

In addition to the network configurations presented in Figure 3, we also considered a case in which no seismic stations were considered (i.e., unconditioned ground shaking) and a case in which only the existing seismic stations are used (see Figure 2). The error (ε_{impact} metric) due to the uncertainty and bias in the ground shaking was calculated for economic losses, number of collapsed buildings and fatalities, as presented in Figure 4.

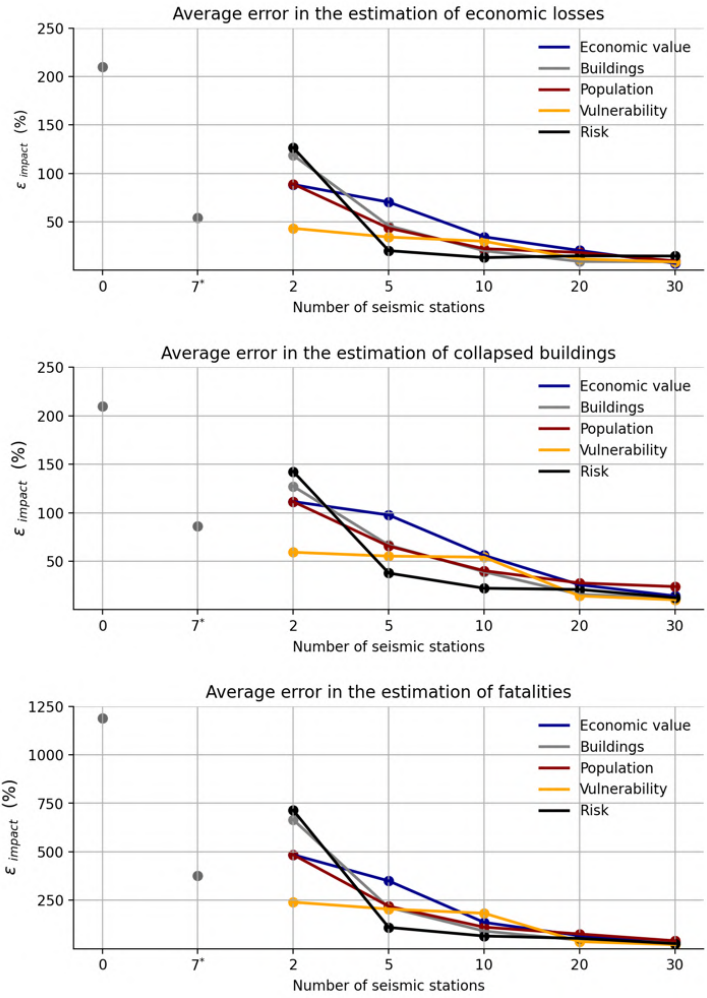

Figure 4. Average error in the estimation of 3 impact metrics (economic losses, number of collapsed buildings and fatalities) considering 6 cases for the number of seismic stations (i.e., no stations, *existing seismic network, and 2, 5, 10, 20 and 30 hypothetical stations and 5 criteria to spatially distribute the hypothetical stations (i.e. proportional to the economic value, number of buildings, population, number of vulnerable buildings and seismic risk)

The results from Figure 9 demonstrate that conditioning ground shaking at strategically allocated seismic stations can significantly reduce the error due to the uncertainty and bias in the ground shaking component. Note that simply including 2 stations in the region can already reduce the error by half, if those 2 stations have been included in locations where the most vulnerable buildings exist. Our results indicate that the most beneficial criterion to distribute stations, that is, allocating them according to the current seismic risk, leads to the lowest error once at least 5 stations are considered. This is a rather expected outcome given that this criterion considers not just the vulnerability and value/quantity of the building stock, but also the associated earthquake hazard and soil conditions. We further investigated why this criterion did not lead to satisfactory results when only two stations were considered. As depicted in Figure 8, this criterion allocates 1 of the 2 stations in a large municipality Northeast of Lisbon, where the seismic hazard is especially high due to the proximity to the Lower Tagus Valley faults and the presence of soft soils. While this station contributes to reducing the error at this municipality, it is too far (> 25 km) from all other municipalities to influence the conditioning of the ground shaking. We also note that, depending on the risk metric and distribution criterion, it is possible to achieve lower errors in comparison to the existing network just with more strategically placed sensors. Finally, we also tested a case with 30 hypothetical stations, to demonstrate that beyond 20 stations, there are diminishing benefits further densification spaced stations.

CHAPTER VIII

08.

Earthquake Risk in Portugal

Earthquake Risk in Portugal

The ASSIMILATE project focused on different components of the earthquake risk assessment problem, leading to the development of new exposure datasets, new sets of vulnerability functions, and testing of existing seismic hazard models for the country. For this reason, we considered that it was also relevant to combine all components and investigate the spatial distribution of seismic risk in the country. This information is fundamental to expand the design of the rapid loss assessment system in the country. As described in the previous chapter, in order to maximize the number of sensors, it is fundamental to distribute the available sensors proportional to the seismic risk in the country.

In this chapter, the assessment of earthquake risk was performed using the Probabilistic Event-based Risk calculator of the OpenQuake-engine (Silva et al. 2014c). This calculator generates a large number of stochastic event sets (SES) using the probabilistic seismic hazard model. We used the hazard model described in Section 3, and generated 100,000 SESs with a one-year duration, randomly sampling different branches of the source model and ground motion logic tree according to the associated weights. For each event in the SES, a ground motion field was generated, considering both the spatial and inter-period correlation in the ground motion residuals using the correlation models from Jayaram and Baker (2010) and Goda and Atkinson (2009), respectively. The

ground shaking at the location of each asset was combined with the associated vulnerability functions and exposure information to compute the expected loss for each event in the SES. These results were used to compute event loss tables, loss exceedance curves and average annualised losses.

Fig. 1 presents the average annualised results aggregated at the district level for five risk metrics: economic losses, buildings with complete damage (or lost), built-up area lost, fatalities, and population left homeless.These results indicate that most of the earthquake risk in Portugal is concentrated in the districts of Lisbon, Setúbal, Santarém, Faro (i.e., Algarve) and in the Azores islands. This trend is due to the significant seismic hazard in these regions, associated with a high concentration of buildings, population, and economic value (see Chapter 2).

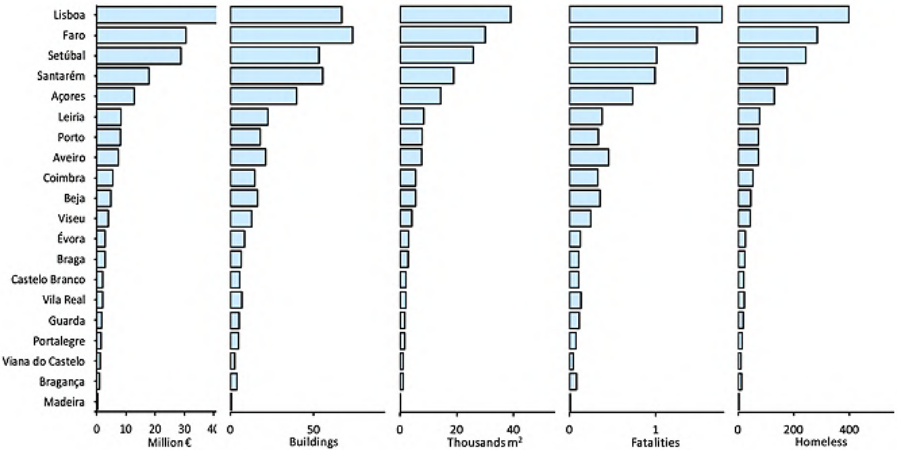

Figure 1. Average annualised results aggregated at the district level for five risk metrics (in this order): economic losses, buildings with complete damage, built-up area lost, fatalities and population left homeless

Figures 2 to 5 present four annualized risk metrics at the second administrative level (i.e., concelho). We note that the risk calculations were performed at a finer resolution (i.e., freguesia), but we decided to aggregate the results at a coarser division for the sake of clarity. The spatial pattern of the risk metrics indicates a higher potential for losses in the Southwest of the country, the Lower Tagus Valley, and the Azores Archipelago.

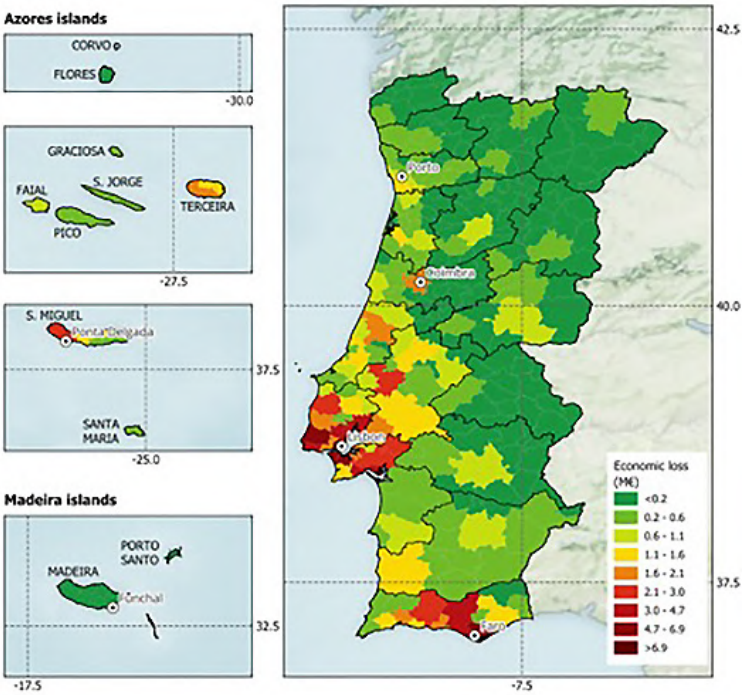

Figure 2. Average annualised economic losses at the second administrative division (i.e., concelho)

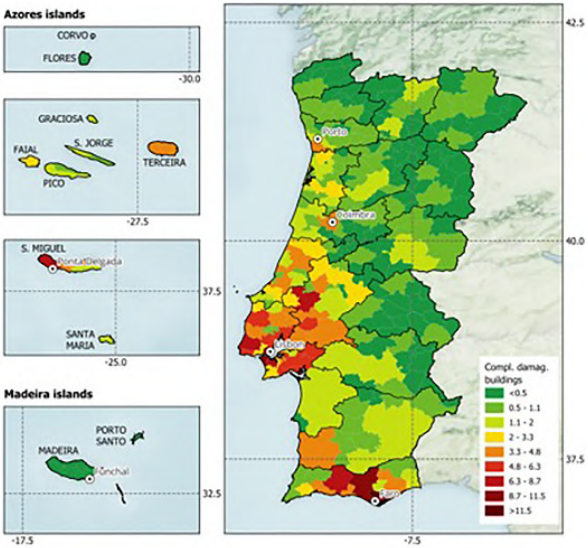

Figure 3. Average annualised number of buildings with complete damage at the second administrative division (i.e., concelho)

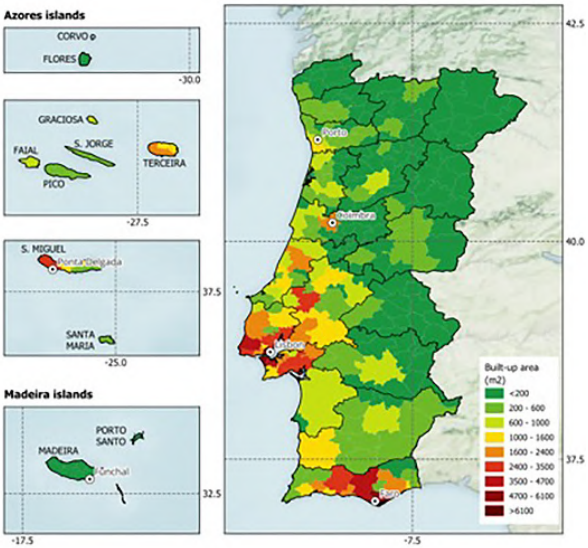

Figure 4. Average annualised loss of built up areaat the second administrative division (i.e., concelho)

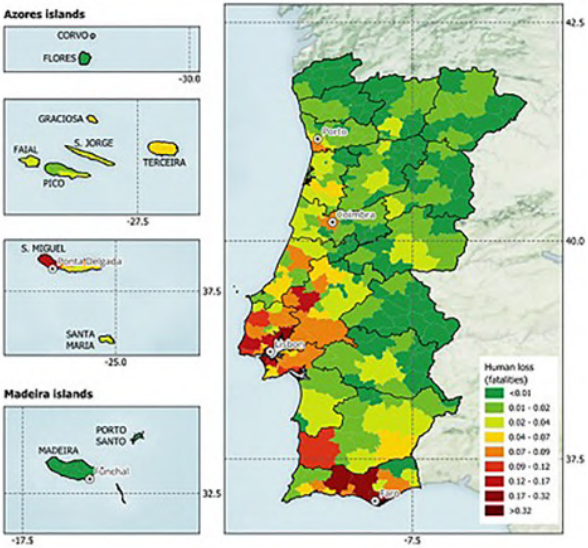

Figure 5. Average annualised human losses at the second administrative division (i.e., concelho)

Table 1 summarizes the selected earthquake risk metrics at the national level, in terms of average annualised losses (AAL). The AAL has also been normalized by the total exposed values to evaluate the average annualised loss ratio (AALR).

Table 1. Summary of the main earthquake risk metrics for Portuga.

Loss type	AAL	R (‰)
Total losses (M€)	187.76	0.211
Human losses	16.08	0.002
Built-up area lost (m^2)	82348	0.099
Buildings lost	448	0.117
Population left homeless	1791	0.173

The economic losses were disaggregated based on the main types of construction and component (structural/nonstructural components and contents), as illustrated in Fig 3. More than half of the economic losses are due to damage in the reinforced concrete building stock, partially due to the fact that a third of these buildings were built before the introduction of the first modern seismic regulation in Portugal (i.e. 1983), but mostly due to the higher costs in comparison with the other typologies. In fact, when these losses are normalized by the economic value, it is clear that unreinforced masonry and adobe have a higher likelihood to suffer damage due to earthquakes.

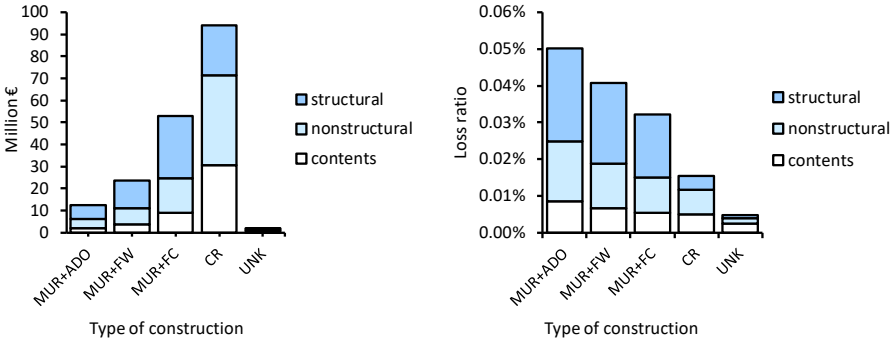

Figure 3. Distribution of the average annual economic losses (left) and loss ratios (right) for different types of construction and components

In comparison with past studies, Silva et al. (2014) estimated an average annual loss of 288M EUR, while Sousa (2006) indicated an annual loss of 257M EUR, both studies only considering the residential building stock. These estimates are considerably higher than the annual loss proposed herein (188M EUR, in particular considering that the present study also covers commercial and industrial facilities, and losses due to damage to contents. One of the reasons for this reduction is the lower seismic hazard, especially for the Northeast of the country whose hazard is below 0.1g (in terms of PGA) for the

475 years return period. The direct comparison of the vulnerability functions for 4 building classes presented in these studies also show a higher vulnerability for the past studies. Finally, it is also worth mentioning that despite the increase in the number of buildings from 2011 to 2021, the newer construction was assumed to follow modern design regulations, whose vulnerability is considerably lower. The AAL indicated by the work of Sousa and Costa (2016) (147M EUR) is more in line with the values presented herein, though again only the residential building stock was considered. A thorough comparison between these studies was not possible due to the fact the individual components were not available for additional analysis. These discrepancies highlight the need to perform seismic risk assessment using open-source tools and openly accessible models to allow the scientific community to further scrutinize each component of the model and reproduce the risk results presented herein under the same assumptions.

CHAPTER IX

09.

Conclusions and main achievements

Conclusions and main achievements

During 34 months, the research team of the ASSIMILATE project investigated critical issues and proposed innovative models and methods to better understand the seismic vulnerability and risk of the Portuguese building stock using low-cost sensors and machine learning, and defined a strategy to build a rapid loss assessment system for the district of Lisbon, that can be expanded to other parts of the country. The exposure model developed for the residential building stock using the 2021 Building Census data estimated a replacement cost of approximately 905 billion EUR, which is about 3.7 times the 2022 Portuguese gross domestic product. The majority of the building stock is located in the Metropolitan Area of Lisbon and Porto, with the seismic hazard (in terms of PGA) in the former area above 0.15g for the 475 years return period. This new exposure model developed within this project highlights areas where additional risk studies should be performed, or where systems to rapidly assess earthquake impact should be deployed.

This project proposed for the first time vulnerability functions defined in terms of period elongation, as opposed to conventional intensity measures such as peak ground acceleration or spectral acceleration. This new approach to estimate building damage has the potential to considerably decrease uncertainty and bias due to the possibility to explicitly account for changes in the structural

integrity of the asset. We covered the most mid-rise reinforced concrete structures in the country, which are the typologies in which variations in the period vibration will be more noticeable. Moreover, more than half of the population live in this type of construction. For the unreinforced masonry building stock, we developed 3D complex numerical models to develop fragility functions to estimate damage and fatalities. According to recent literature, these typologies are typically responsible for most of the fatalitiesin destructive earthquakes.

On the ground shaking counterpart, we developed a machine learning ground motion model using all of the ground motion recordings from the Portuguese and Spanish ground motion databases. This is one of the first models developed for the region using stochastic simulations, whose parameters were specifically developed for inland and offshore events for Portugal. The developed model was compared with the existing ground motion models for other stable continental regions as well as the available models for low--to-moderate hazard regions in Europe, some of which have been used in the past in seismic hazard and risk analysis for the country. In general, we noted that most models tend to underestimate the ground shaking for the offshore events, and overestimate for the inland events. This trend could mean that the seismic hazard due to inland seismicity might be overestimated, while the contribution of the offshore events to the national seismic hazard and risk could be underestimated.

Using these models, we investigated the benefits that seismic monitoring might bring to a region in terms of error and bias reduction. Due to the lack of strong ground shaking for Portugal, we tested this hypothesis using recorded ground shaking from the 1999 M7.7 Chi-Chi (Taiwan) earthquake. Our results indicated a median error below 25% in the estimation of the event bias (or inter-event residual) when at least 25 stations are considered. For PGA, a significant reduction in the ground shaking estimation error was also observed. This observation highlights that even in regions with dense seismic networks such as Taiwan, significant shaking uncertainties remain.

Then, to extend this study to our region of interest (District of Lisbon), we evaluated how seismic monitoring can reduce the error in the estimation of impact metrics such as damage buildings, fatalities and economic losses. We concluded that including at least 10 stations for a region as large as the district of Lisbon (~2,800 km2) can reduce the estimation error by one order of magnitude, compared with the case in which no stations are used (i.e., unconditioned ground shaking). It was also possible to observe that distributing the seismic stations proportional to the number of vulnerable buildings or the estimated earthquake risk led to the most evident reduction in the error. In contrast, allocating seismic stations based only on the economic value of the building stock, number of buildings, or population count led to larger errors, unless an excessive number of stations was used.

Finally, we combined these components together to calculate earthquake risk in the entire territory. Such outcome is useful to inform the development of risk mitigation strategies for the country, but also to understand where seismic sensors should be deployed to rapidly estimate ground shaking (and consequently the associated impact), as previously described. In terms of earthquake risk, the estimated average annual economic losses of 188M EUR are considerable for the country. To put in perspective, this loss is equivalent to one third of the construction cost of the new hospital in Lisbon, one of the largest in the country. The human impact (average annual human losses) is relatively low, mostly due to the fact that the building stock is mostly comprised of structures with 1-2 storeys, which tend to have lower collapse and fatality rates. The seismic risk map highlights the Lower Tagus Valley, the South of Portugal, and the Azores islands as high-risk regions, with adobe and unreinforced masonry typologies identified as the most vulnerable.

The results of this project have been presented in peer-reviewed articles and national/international conferences, as listed below. Moreover, the research team met on several occasions with stakeholders and partners of this project including the City Hall of Lisbon, the Association of Municipalities of Lisbon, the National Laboratory of Civil Engineering, the Portuguese Authority for Civil Protection, Safehub Inc and the Global Earthquake Model Foundation.

Peer-reviewed publications

1. Silva V, Taherian A, Oliveira CS. (2022). Earthquake early warning for Portugal: Part 1 - Where does it matter? Bulletin of Earthquake Engineering, 20:5545–5565. https://doi.org/10.1007/s10518-022-01400-4
2. Silva V, Taherian A, Oliveira CS. (2023). Earthquake early warning for Portugal: Part 2 - Where is it beneficial? Bulletin of Earthquake Engineering, 20:5545–5565. https://doi.org/10.1007/s10518-023-01715-w
3. Lovon H, Silva V, Vicente R, Ferreira TM (2023). Seismic Vulnerability Assessment of Portuguese Masonry Buildings. Structures, 55:853-865, https://doi.org/10.1016/j.istruc.2023.06.083
4. Lovon H, Silva V, Vicente R, Ferreira T (2021). Development of a seismic vulnerability model for the estimation of fatalities. Earthquake Engineering and Structural Dynamics, in review.
5. Amir Taherian, Vitor Silva, Petros Kalakomas, Romeu Vicente. (2024). Earthquake Ground Motion Prediction Model for Southwest Iberia. Bulletin of Seismological Society of America, in review.
6. Silva V, Wald S, Taherian A (2024). Benefits of Seismic Monitoring
   for Ground Shaking Estimation and Loss Assessment. Bulletin of Seismological Society of America, in review.
7. Lopes G, Silva V, Costa C, Vicente R, Oliveira CS (2024). Advancing the Understanding of Earthquake Risk in Portugal. Bulletin of Earthquake Engineering, in review.

Publication in International Conferences

1. Shafie R, Varum H, Silva V, Melo J, Romao X (2023). Vulnerability Assessment of Reinforced Concrete (RC) Structures based on Modal Parameters. Proceedings of the XLIV Ibero-Latin American Congress on Computational Methods in Engineering, ABMEC, Porto, Portugal.
2. Silva V, Taherian A, Vicente R (2023). Designing Equitable and Dynamic Rapid Earthquake Loss Assessment Systems. 14th International Conference on Applications of Statistics and Probability in Civil Engineering, Dublin, Ireland.
3. Lovon H, Silva V, Vicente R, Ferreira T (2022). Development of Analytical Fatality Vulnerability Functions for Masonry Buildings in Portugal. 3rd European Conference on Earthquake Engineering and Seismology, Bucharest, Romania.
4. Martins L, Silva V (2022). A Single Deep Learning Model for Portfolio Risk Analysis. 3rd European Conference on Earthquake Engineering and Seismology, Bucharest, Romania.
5. Melo J, Triantafyllidis Z, Rush D, Bisby L, Rossetto R, Arêde A, Varum H, Ioannou I (2022) Experimental assessment of post-fire retrofitted RC columns tested under cyclic loading. 3rd European Conference on Earthquake Engineering & Seismology, 3ECEES - Bucharest, Romania, 4-9 setembro 2022.

Publication in National Conferences

1. Silva V, Oliveira CS, Matias L, Carrilho F (2022). Earthquake Early Warning for Portugal:Where, Why and How Much. 12º Congresso Nacional de Sismologia e Engenharia Sísmica, Lisbon, Portugal.
2. Silva V (2022). The Promise of New Technologies in the Evaluation of Earthquake Risk: Hype or Hope? 12º Congresso Nacional de Sismologia e Engenharia Sísmica, Lisbon, Portugal.
3. Silva V, Taherian A, Vicente R (2024). The Benefits of Low-cost Sensors in Rapid Earthquake Loss Assessment. Proceedings of the 13th

Conference in Earthquake Engineeing and Seismology - SISMICA, Guimaraes, Portugal.

4. Shafie R, Varum H, Silva V, Melo J, Romao X (2024). Damage Assessment of Reinforced Concrete (RC) Structures based on Modal Parameters. Proceedings of the 13th Conference in Earthquake Engineeing and Seismology - SISMICA, Guimaraes, Portugal.
5. Lopes G, Silva V, Costa C, Vicente R, Oliveira CS (2024). Enhancing Earthquake Risk Assessment in Portugal: a Comprehensive Analysis. Proceedings of the 13th Conference in Earthquake Engineeing and Seismology - SISMICA, Guimaraes, Portugal.
6. Shafie R, Varum H, Silva V, Melo J, Romao X (2023). Damage detection of Reinforced Concrete (RC) Structures based on Period Elongation. The 5th Doctoral Congress in Engineering, DCE23, Porto, Portugal.

CHAPTER X

References

Abadi M, Agarwal A, Barham P, et al (2016) TensorFlow: Large-Scale Machine Learning on Heterogeneous Distributed Systems

Abeling S, Ingham JM. (2020). Volume loss fatality model for as-built and retrofitted clay brick unreinforced masonry buildings damaged in the 2010/11 Canterbury earthquakes. Structures. 24:940-954. doi:10.1016/j.istruc.2020.02.014

Abrahamson NA, Youngs RR (1992). A stable algorithm for regression analyses using the random effects model. Bull Seismol Soc Am 82(1):505–510. doi.org/10.1785/BSSA0820010505

Aki K (1972) Earthquake mechanism. Tectonophysics 13:423–446. https://doi.org/10.1016/0040-1951(72)90032-7

Akkar S, Bommer JJ (2010) Empirical equations for the prediction of PGA, PGV and spectral accelerations in Europe, the Mediterranean Region and the Middle East. Seism Res Lett 81:195–206. https://doi.org/10.1785/gssrl.81.2.195

Akkar S, Sandikkaya MA, Bommer JJ (2014). Empirical Ground-Motion Models for Point- and Extended- Source Crustal Earthquake Scenarios in Europe and the Middle East. Bull Earthquake Eng 12, 359–387, doi.org/10.1007/s10518-013-9461-4

Allen TI (2012) Stochastic ground-motion prediction equations for southeastern Australian earthquakes using updated source and attenuation parameters

Ambraseys NN, Douglas J, Sarma SK, Smit PM (2005) Equations for the estimation of strong ground motion from shallow crustal earthquakes using data from Europe and the Middle East: horizontal peak ground acceleration and spectral acceleration. Bull Earthq Eng 3:1–53. https://doi.org/10.1007/s10518-005-0183-0

Assatourians K, Atkinson GM (2007). Modeling Variable-Stress Distribution with the Stochastic Finite-Fault Technique. Bulletin of the Seismological Society of America 97:1935–1949. https://doi.org/10.1785/0120060203

Atkinson GM, Assatourians K (2014). Implementation and Validation of EXSIM (A Stochastic Finite Fault Ground Motion Simulation Algorithm) on the SCEC Broadband Platform. Seismological Research Letters, 86 (1): 48–60. doi: https://doi.org/10.1785/0220140097

Atkinson GM, Boore DM (1995) Ground-motion relations for eastern North America. Bulletin of the Seismological Society of America 85:17–30. https://doi.org/10.1785/BSSA0850010017

Atkinson GM, Boore DM (2006) Earthquake Ground-Motion Prediction Equations for Eastern North America. Bulletin of the Seismological Society of America 96:2181–2205. https://doi.org/10.1785/0120050245

Atkinson GM, Boore DM (2006) Earthquake Ground-Motion Prediction Equations for Eastern North America. Bulletin of the Seismological Society of America 96:2181–2205. https://doi.org/10.1785/0120050245

Auer P, Burgsteiner H, Maass W (2008) A learning rule for very simple universal approximators consisting of a single layer of perceptrons. Neural Networks 21:786–795. https://doi.org/https://doi.org/10.1016/j.neunet.2007.12.036

Baker, J. (2011) Conditional Mean Spectrum: Tool for Ground-Motion Selection. Journal of Structural Engineering, 137(3): p. 322-331. DOI: 10.1061/(ASCE)ST.1943-541X.0000215

Boore DM (1983) Stochastic simulation of high-frequency ground motions based on seismological models of the radiated spectra. Bulletin of the Seismological Society of America 73:1865–1894. https://doi.org/10.1785/BSSA07306A1865.

Boore DM (2003) Simulation of Ground Motion Using the Stochastic Method. Pure Appl Geophys 160:635–676. https://doi.org/10.1007/PL00012553

Brune JN (1970) Tectonic stress and the spectra of seismic shear waves from earthquakes. Journal of Geophysical Research (1896-1977) 75:4997–5009. https://doi.org/https://doi.org/10.1029/JB075i026p04997

Calvi GM, Pinho R, Crowley H (2006). State-of-the-knowledge on the period elongation of RC buildings during strong ground shaking, 1st European conference on earthquake engineering and seismology. Geneva, Switzerland.

Carrilho F, Custódio S, Bezzeghoud M, Oliveira CS, Marreiros C, Vales D, Alves P, Pena A, Madureira G, Escuer M, Silveira G, Corela C, Matias L, Silva M, Veludo I, Dias N, Loureiro A, Borges J, Caldeira B, Wachilala P, Fontiela J (2021). The Portuguese National Seismic Network—Products and Services. Seismological Research Letters 92 (3): 1541–1570. doi: https://doi.org/10.1785/0220200407

Cauzzi C, Faccioli E, Vanini M, Bianchini A (2015). Updated predictive equations for broadband (0.01–10 s) horizontal response spectra and peak ground motions, based on a global dataset of digital acceleration records. Bull Earthquake Eng 13, 1587–1612, doi.org/10.1007/s10518-014-9685-y

Ceferino L, Kiremidjian A, Deierlein G. (2018). Regional Multiseverity Casualty Estimation Due to Building Damage following a Mw 8.8 Earthquake Scenario in Lima, Peru. Earthquake Spectra. 34(4):1739-1761. doi:10.1193/080617EQS154M

Chan CH, Ma KF, Shyu JBH, Lee YT, Wang YJ, Gao JC, Yen YT, Rau RJ (2020). Probabilistic seismic hazard assessment for Taiwan: TEM PSHA2020. Earthquake Spectra. 36:137-159. doi:10.1177/8755293020951587

Chao SH, Chiou B, Hsu CC, Lin OS (2020). A horizontal ground-motion model for crustal and subduction earthquakes in Taiwan. Earthquake Spectra., 36(2):463-506. doi:10.1177/8755293019891711

Chen CT, Chang SC, Wen KL (2017). Stochastic ground motion simulation of the 2016 Meinong, Taiwan earthquake. Earth, Planets and Space. 69. 10.1186/s40623-017-0645-z

Cotton F, Archuleta R, Causse M (2013) What is Sigma of the Stress Drop? Seismological Research Letters 84:42–48. https://doi.org/10.1785/0220120087

Cremen G, Galasso C, Zuccolo E (2022) Investigating the potential effectiveness of earthquake early warning across Europe. Nature Communications 13, 639

Crowley H, Polidoro B, Pinho R, Van Elk J (2017). Framework for developing fragility and consequence models for local personal risk. Earthquake Spectra.;33(4):1325-1345. doi:10.1193/083116EQS140M

Crowley H, Stafford PJ, Bommer JJ (2008). Can Earthquake Loss Models be Validated Using Field Observations?, Journal of Earthquake Engineering, 12:7, 1078-1104, DOI: 10.1080/13632460802212923

D'Amico S, Akinci A, Malagnini L (2012). Predictions of high--frequency ground-motion in Taiwan based on weak motion data. Geophysical Journal International, 189 (1): 611–628, https://doi.org/10.1111/j.1365-246X.2012.05367.x

Danciu L, Nandan S, Reyes C, Basili R, Weatherill G, Beauval C, Rovida A, Vilanova S, Sesetyan K, Bard PY, Cotton F, Wiemer S, Giardini D (2021). The 2020 update of the European Seismic Hazard Model: Model Overview. EFEHR Technical Report 001, v1.0.0, https://doi.org/10.12686/a15

Delavaud E, Cotton F, Akkar S, et al (2012) Toward a ground-motion logic tree for probabilistic seismic hazard assessment in Europe. J Seismol 16:451–473. https://doi.org/10.1007/S10950-012-9281-Z/TABLES/15

Derras B, Bard PY, Cotton F (2014) Towards fully data driven ground-motion prediction models for Europe. Bulletin of Earthquake Engineering 12:495–516. https://doi.org/10.1007/s10518-013-9481-0

Dhanya J, Raghukanth STG (2018) Ground Motion Prediction Model Using Artificial Neural Network. Pure Appl Geophys 175:1035–1064. https://doi.org/10.1007/s00024-017-1751-3

Diaz J, Gallart J, Carbonell R (2016) Moho topography beneath the Iberian-Western Mediterranean region mapped from controlled-source and natural seismicity surveys. Tectonophysics 692:74–85. https://doi.org/https://doi.org/10.1016/j.tecto.2016.08.023

Edwards B, Fäh D (2013) A Stochastic Ground Motion Model for Switzerland. Bulletin of the Seismological Society of America 103:78–98. https://doi.org/10.1785/0120110331

Engler DT, Worden CB, Thompson EM, Jaiswal KS (2022). Partitioning Ground Motion Uncertainty When Conditioned on Station Data. Bulletin of the Seismological Society of America, 112(2), 1060–1079. DOI: https://doi.org/10.1785/0120210177

Erdik M, Fahjan Y, Orguz O, Alcik H, Mert A, Gul M (2003). Istanbul earthquake rapid response and the early warning system. Bull Earthq Eng. 1(1):157-163

Erduran E, Lang D, Lindholm C, Toma-Danila D, Balan S, Ionescu V, Aldea A, Vacareanu R, Neagu C (2012). Real-time earthquake damage assessment in the Romanian-Bulgarian Border region. In: Proceedings of the 15Th World Conference on Engineering; Lisbon, Portugal

FEMA (2018) P-58-1: Seismic Performance Assessment of Buildings. Volume 1 – Methodology. Vol 1.

Fiorini E, Borzi B, Iaccino R (2012). Real Time damage scenario: case study for the L'Aquila earthquake. Proceedings of the 15th World Conference on Earthquake Engineering, Lisbon, Portugal, 2012

Gallipoli MR et al. (2020). Structural health monitoring of the Ferrara University before and after the 2012 Emilia (Italy) earthquake, and after the damage repairs. Structural Health Monitoring,. 19(3): p. 838-853

Goda K, Atkinson GM (2009). Probabilistic characterization of spatially correlated response spectra for earthquakes in Japan. Bulletin of the Seismological Society of America; 99(5): 3003–3020

Goda K, Hong HP (2008) Spatial correlation of peak ground motions and response spectra. Bulletin of the Seismological Society of America 98(1):354–365

Grant DN, Dennis J, Sturt R, et al. (2021). Explicit modelling of collapse for Dutch unreinforced masonry building typology fragility functions. Bulletin of Earthquake Engineering. 2021;19(15):6497-6519. doi:10.1007/S10518-020-00923-Y/FIGURES/6

Hanks TC, McGuire RK (1981) The character of high-frequency strong ground motion. Bulletin of the Seismological Society of America 71:2071–2095. https://doi.org/10.1785/BSSA0710062071

Hartzell SH (1978) Earthquake aftershocks as Green's functions. Geophys Res Lett 5:1–4. https://doi.org/https://doi.org/10.1029/GL005i001p00001

Haykin S (2009) Neural Networks and Learning Machines. Pearson, New Jersey

Hoshiba M, Iwakiri K, Hayashimoto N, et al. (2011). Outline of the 2011 off the Pacific coast of Tohoku earthquake (Mw 9.0) earthquake early warning and observed seismic intensity. Earth Planets Space. 63:547-551.

Indirli M, Kouris LAS, Formisano A, Borg RP, Mazzolani FM. (2013). Seismic damage assessment of unreinforced masonry structures after the Abruzzo 2009 earthquake: The case study of the historical centers of L'Aquila and Castelvecchio Subequo. International Journal of Architectural Heritage;7(5):536-578. doi:10.1080/15583058.2011.654050

Jaiswal K, Wald D (2010). Development of a semi-empirical loss model within the USGS Prompt Assessment of Global Earthquakes for Response (PAGER) System. Proceedings of the 9th US and 10th Canadian Conference on Earthquake Engineering, Toronto, Canada

Jaiswal K, Wald D (2013). Estimating Economic Losses from Earthquakes Using an Empirical Approach. Earthquake Spectra 2013 29:1, 309-324

Jayaram N, Baker JW. (2010). Correlation model for spatially distributed ground-motion intensities. Earthquake Engineering and Structural Dynamics, 38(15):1687-1708

Johnston AC (1996) Seismic moment assessment of earthquakes in stable continental regions?III. New Madrid 1811-1812, Charleston 1886 and Lisbon 1755. Geophys J Int 126:314–344. https://doi.org/10.1111/j.1365-246X.1996.tb05294.x

Joshi A, Kuo CH, Dhibar P, Sandeep, Sharme ML, Wen KL, Lin CM (2015). Simulation of the records of the 27 March 2013 Nantou Taiwan earthquake using modified semi-empirical approach. Natural Hazards. 78. 10.1007/s11069-015-1754-2

Kalakonas P, Rao A, Mouyiannou A, Silva V (2020). Exploring the Impact of Epistemic Uncertainty on Regional Probabilistic Seismic Risk Assessment. Natural Hazards. https://doi.org/10.1007/s11069-020-04201-7

Kalakonas P, Silva V (2022) Seismic vulnerability modelling of building portfolios using artificial neural networks. Earthq Eng Struct Dyn 51:310–327. https://doi.org/https://doi.org/10.1002/eqe.3567

Kotha SR, Weatherill G, Cotton F (2020). A regionally adaptable ground motion model for shallow crustal earthquakes in Europe. Bulletin of Earthquake Engineering. 18:4091–4125

Lovon H, Silva V, Vicente R, Ferreira TM, Costa AA. (2021). Characterisation of the masonry building stock in Portugal for earthquake risk assessment. Eng Struct; 233:111857. doi:10.1016/j.engstruct.2021.111857

Lovon H, Silva V, Vicente R, Ferreira TM. (2022). Seismic vulnerability Assessment of Portuguese masonry buildings. Structures. Published online.

Maio R, Estêvão JMC, Ferreira TM, Vicente R. (2020). Cost-benefit analysis of traditional seismic retrofitting strategies integrated in the renovation of stone masonry buildings. Eng Struct.;206:110050. doi:10.1016/j.engstruct.2019.110050

Marano KD, Hearne M, Jaiswal KS, Thompson EM, Worden CB, Wald DJ (2023). ShakeMap Atlas 4.0 and AtlasCat: An Archive of the Recent and the Historical Earthquake ShakeMaps, and Impacts for Global Hazard Analyses and Loss Model Calibration, Seismol. Res. Lett. XX, 1–21,doi: 10.1785/0220220324

Martins L, Silva V (2020). Development of a Fragility and Vulnerability Model for Global Seismic Risk Assessment. Bulletin of Earthquake Engineering, https://doi.org/10.1007/s10518-020-00885-1

McBride SK, Smith H, Morgoch M, Sumy D, Jenkins M, Peek L, Bostrom A, Baldwin D, Reddy E, Groot R, Becker J, Johnston D, Wood M (2022). Evidence-based guidelines for protective actions and earthquake early warning systems. Geophysics 87, no. 1, 1–79, doi: 10.1190/ geo2021-0222.1

Motazedian D, Atkinson GM (2005). Stochastic Finite-Fault Modeling Based on a Dynamic Corner Frequency. Bulletin of the Seismological Society of America 95:995–1010. https://doi.org/10.1785/0120030207

Okada S (1996). Description for indoor space damage degree of building in earthquake. In: Proceedings of the 11th World Conference on Earthquake Engineering

Pagani M, Monelli D, Weatherill G, Danciu L, Crowley H, Silva V, Henshaw P, Butler L, Nastasi M, Panzeri L, Simionato M, Vigano D (2014). OpenQuake Engine: An open hazard (and risk) software for the Global Earthquake Model. Seismological Research Letters, (85)3:692-702. doi.org/10.1785/0220130087

Rietbrock A, Strasser F, Edwards B (2013) A Stochastic Earthquake Ground Motion Prediction Model for the United Kingdom. Bulletin of the Seismological Society of America 103:57–77. https://doi.org/10.1785/0120110231

Roumelioti Z, Beresnev IA (2003). Stochastic finite-fault modeling of ground motions from the 1999 Chi-Chi, Taiwan, earthquake: application to rock and soil sites with implications for nonlinear site response, Bull. seism. Soc. Am., 93, 1691–1702

Shome, N. and Cornell, C.A. (1999) Probabilistic seismic demand analysis of nonline-ar structures, Technical Report RMS-35, Stanford University.

Silva V (2016). Critical Issues in Earthquake Scenario Loss Modelling. Journal of Earthquake Engineering, 20(8):1322-1341. doi.org/10.1080/13632469.2016.1138172

Silva V, Amo-Oduro D, Calderon A, Costa C, Dabbeek J, Despotaki V, Martins L, Pagani M, Rao A, Simionato M, Viganò D, Yepes-Estrada C, Acevedo A, Crowley H, Horspool N, Jaiswal K, Journeay M, Pittore M (2020). Development of a Global Seismic Risk Model. Earthquake Spectra, doi.org/10.1177/8755293019899953

Silva V, Crowley H, Varum H (2014) Seismic risk assessment for mainland Portugal. Bulletin of Earthquake Engineering. https://doi.org/10.1007/s10518-014-9630-0

Silva V, Crowley H, Varum H, Pinho R. (2014). Seismic risk assessment for mainland Portugal. Bulletin of Earthquake Engineering.;13(2):429-457. doi:10.1007/s10518-014-9630-0

Silva V, Horspool N (2019). Combining USGS ShakeMaps and the OpenQuake-engine for damage and loss assessment. Earthquake Engineering and Structural Dynamics. 48(6):634-652

Silva V, Marques M, Castro JM, Varum H (2015). Development and Application of a Real-time Loss Estimation Framework for Portugal. Bulletin of Earthquake Engineering, 13:2493–2516. doi.org/10.1007/s10518-015-9743-0

Silva V, Taherian A, Oliveira CS. (2022). Earthquake early warning for Portugal: Part 1 - Where does it matter? Bulletin of Earthquake Engineering, 20:5545–5565. https://doi.org/10.1007/s10518-022-01400-4

Silva V, Taherian A, Oliveira CS. (2023). Earthquake early warning for Portugal: Part 2 - Where is it beneficial? Bulletin of Earthquake Engineering, 20:5545–5565. https://doi.org/10.1007/s10518-023-01715-w

Silva, V. (2019) Uncertainty and correlation in seismic vulnerability functions of building classes. Earthquake Spectra. DOI: 10.1193/013018eqs031m

So E. (2012). Derivation of globally applicable casualty rates for use in earthquake loss estimation models. In: 15th World Conference on Earthquake Engineering

So E. (2016). Estimating Fatality Rates for Earthquake Loss Models. Springer International Publishing;. doi:10.1007/978-3-319-26838-5

Sousa ML, Costa AC (2016) Evolution of earthquake losses in Portuguese residential building stock. Bulletin of Earthquake Engineering 14:2009–2029. https://doi.org/10.1007/s10518-015-9809-z

Sousa, M. (2006). Risco sísmico em Portugal continenal. Ph.D. Thesis, Instituto Superior Técnico, Lisbon, Portugal

Spence R (2007) LESSLOSS Report 2007/07 - Earthquake Disaster Scenario Predictions & Loss Modelling for Urban Areas

Spence R (2021), So E. Why Do Buildings Collapse in Earthquakes? 1st ed. John Wiley & Sons, Ltd

Stafford PJ (2014) Crossed and Nested Mixed Effects Approaches for Enhanced Model Development and Removal of the Ergodic Assumption in Empirical Ground Motion Models. Bulletin of the Seismological Society of America 104:702–719. https://doi.org/10.1785/0120130145

Taherian A, Silva V, Kalakonas P, Vicente R (2024). An Earthquake Ground Motion Model for Southwest Iberia. Bulletin Seismological Society of America (in review). Available at: https://shorturl.at/giqJP

Vidal F, Navarro M, Caballero X, Enomoto T (2014). Changes in Dynamic Characteristics of Lorca Rc Buildings from Pre- and Post-Earthquake Ambient Vibration Data. Vol. 12,. doi:10.1007/s10518-013-9489-5.

Vilanova SP, Fonseca JFBD, Oliveira CS (2012) Ground Motion Models for Seismic Hazard Assessment in Western Iberia: Constraints from Instrumental Data and Intensity Observations. Bulletin of the Seismological Society of America 102:169–184. https://doi.org/10.1785/0120110097

Vilanova SP, Fonseca JFBD. (2007). Probabilistic seismic-hazard assessment for Portugal. Bulletin of the Seismological Society of America.;97(5):1702-1717. doi:10.1785/0120050198

Wald DJ (2020). Practical limitations of earthquake early warning. Earthquake Spectra, 36 (3), pp. 1412-1447.

Wald DJ, Seligson HA, Rozelle J, Burns J, Marano K, Jaiswal KS, Hearne M, Bausch D (2020). A domestic earthquake impact alert protocol based on the combined USGS PAGER and FEMA Hazus loss estimation systems, Earthquake Spectra 36, 164–182, doi: 10.1177/8755293019878187.

Wald, DJ, Lin K, and Quitoriano V (2008). Quantifying and Qualifying USGS ShakeMap Uncertainty: U.S. Geological Survey Open File Report 2008–1238, 26 pp.

Worden CB, Thompson EM, Baker JW, Bradley BA, Luco N, Wald DJ (2018). Spatial and spectral interpolation of ground-motion intensity measure observations, Bulletin Seismological Society of America. 108, 866–875, doi: 10.1785/0120170201.

Wyss M (2004). Real time prediction of earthquake casualties. Disasters and Society-From Hazard Assessment to Risk Reduction, edited by D. Malzahn and T. Plapp, pp. 165-173, Logos, Berlin.

Xie Y, Ebad Sichani M, Padgett JE, DesRoches R (2020) The promise of implementing machine learning in earthquake engineering: A state--of-the-art review. Earthquake Spectra 36:1769–1801. https://doi.org/10.1177/8755293020919419

Yepes-Estrada C, Silva V, Rossetto T, et al. (2016). The Global Earthquake Model Physical Vulnerability Database: https://doi.org/101193/011816EQS 015DP.;32(4):2567-2585. doi:10.1193/011816EQS015DP

Zafarani H, Luzi L, Lanzano G, Soghrat MR (2018) Empirical equations for the prediction of PGA and pseudo spectral accelerations using Iranian strong-motion data. J Seismol 22:263–285. https://doi.org/10.1007/S10950-017-9704-Y/TABLES/2

Zhang W, Iwata T, Irikura K (2010). Dynamic simulation of the 1999 Chi-Chi, Taiwan, earthquake, Journal Geophys. Res., 115, B04305, doi:10.1029/2008JB006201.

Sunt. Temqui occab ipsanis eiur? Parunt.

Ugiti sequiat quatur, quo modistrum con nemperio. Itatemp elitatus es ulparcient.

Puditatem quia invelis tinctem quas dentia cum re reperum volora nos que dignatur? Quidus re occatiam ut voluptaquia sita doluptaspe dit od quiat re preicimolum ium acest posanis accus dolore dignis evelis eos autenis exceatem volupta tiore, cus ut perumquat.

Lupicia plia dolor aut late nes eum latemquist undis duciliqui alit autat aute preptas et pratibus magnimin nis mi, coreheniae. Itatibusa quas secti atquost as excero blam nisciet verspel invenih ilitectae nonsequae pe ero eossi volupta doluptate praes andem sitatet rerferiamus rectatus.

Solessimus eiur, am ipis a volupta temolupici doluptae. Ut auditi dis alibusaero dolorenet ute ne dipsandipic te culpa volecusto dolorum quam fugia videlis aspis alit enihill uptiassit aut volupta tquias sent venit, sustrum debitae mo es id quate pos a iumet, il erunti temporecte sam faccae et quis sus quodit la voloratemost quo est ped mos aut escitisque qui untur, nem ea cus nimin eos rehendelecto voloriores alit faccus ea que culpa dolorporunt voleculpa et aliquasit eium dolor apitis as de nossitate la dolorro dolupta vit et eaquos arum facearchilic temquia eperum dolo evel illaceped minus quae eos dolorpore vita sum quam sum dolorundit fugiae velibusa ducia quidellupic tore, offici illenecte omnissus eum hilitat.

Invenis evelit, tor maximolupta volut fuga. Ut ad ea inci non net la eatemol uptiosa que id molorer chicipis acculparum quas autem nimenes veribus doluptatio te repration parum quossim porrum venderae sa ent places et eroribust, none sitatin enditatur resequam, veligendus, odis etur modita-que ipsandebit am, et, cum nobiscil iunt, officiae nobita dolupita comnimo luptur aut qui culleniatem alit ut eveliate et eos etum sitiorio endae quam sitis audi int, sint quis inis eum et rest eic tem. Nequis et eum re provit is rempor sequat dit estiore pelibusant quibus doluptate pernatem dolorro

risco
universidade de aveiro
risks and sustainability
in construction

U.PORTO
FEUP FACULDADE DE ENGENHARIA
UNIVERSIDADE DO PORTO

fct
Fundação
para a Ciência
e a Tecnologia

FUNDAÇÃO
FERNANDO
PESSOA

REPÚBLICA
PORTUGUESA